DISEASES AND DISORDERS

Prevention of age-related truncation of γ-glutamylcysteine ligase catalytic subunit (GCLC) delays cataract formation

Zongbo Wei[1]†, Caili Hao[1]†, Kazi Rafsan Radeen[1], Ramkumar Srinivasagan[2], Jian-Kang Chen[1], Shruti Sharma[3], Meghan E. McGee-Lawrence[1], Mark W. Hamrick[1], Vincent M. Monnier[4], Xingjun Fan[1]*

A sharp drop in lenticular glutathione (GSH) plays a pivotal role in age-related cataract (ARC) formation. Despite recognizing GSH's importance in lens defense for decades, its decline with age remains puzzling. Our recent study revealed an age-related truncation affecting the essential GSH biosynthesis enzyme, the γ-glutamylcysteine ligase catalytic subunit (GCLC), at aspartate residue 499. Intriguingly, these truncated GCLC fragments compete with full-length GCLC in forming a heterocomplex with the modifier subunit (GCLM) but exhibit markedly reduced enzymatic activity. Crucially, using an aspartate-to-glutamate mutation knock-in (D499E-KI) mouse model that blocks GCLC truncation, we observed a notable delay in ARC formation compared to WT mice: Nearly 50% of D499E-KI mice remained cataract-free versus ~20% of the WT mice at their age of 20 months. Our findings concerning age-related GCLC truncation might be the key to understanding the profound reduction in lens GSH with age. By halting GCLC truncation, we can rejuvenate lens GSH levels and considerably postpone cataract onset.

INTRODUCTION

Cataract, a disease characterized by lens cloudiness, is a leading cause of blindness worldwide. Aging is the primary risk factor, and age-related cataract accounts for the majority of cases (*1*). According to the World Health Organization and the Global Burden of Disease Study in 2020 (*2*), cataracts caused over 15 million of the 33.6 million cases of global blindness in adults aged 50 and older, as well as 78.8 million cases of moderate and severe vision impairment of a total of 206 million cases in the same age group. With the global aging population rapidly increasing, cataract cases are projected to rise substantially.

Now, cataract can be effectively treated through surgery by replacing the clouded lens with an artificial intraocular lens (*3*). However, financial constraints and limited access to health care for surgical treatment profoundly affect a large population. In addition, cataract surgery can lead to complications such as posterior capsule opacification (PCO), also known as secondary cataract, which is the most common complication following cataract surgery. Severe PCO may require further surgery, such as a Yttrium aluminum garnet (YAG) laser capsulotomy, which can introduce additional complications, such as increasing transient intraocular pressure, lens subluxation and dislocation, retinal detachment and lens pitting, exacerbation of local endophthalmitis, and free-floating fragments (*4*–*7*).

To address this challenge, the best option is to prevent or delay cataract formation. Delaying the onset of cataracts by 10 years could markedly improve the quality of life for more than half of the patients by reducing the need for surgery (*8*). Preventive measures for age-related cataracts can be complex due to multiple risk factors. However, targeting common risk factors, such as reducing ultraviolet (UV) exposure and quitting smoking, has been found to effectively delay cataract onset, offering promising outcomes (*9*, *10*).

During lens aging, various biological, biochemical, and physiological changes occur, contributing to insult to the lens proteins and cataract formation (*11*, *12*). These changes include impaired chaperone function of crystallin proteins (*13*, *14*), accumulation of posttranslational modifications [e.g., glycation (*12*, *15*), deamidation (*16*, *17*), sumoylation (*18*), and isomerization (*19*)], elevated lipid peroxidation(*20*, *21*), and increased oxidative stress (*22*). Reactive oxygen species accumulation is a recognized crucial factor in lens aging and cataract formation (*23*, *24*).

The lens is a unique tissue in that its proteins and lipids do not turnover with age, and yet it maintains transparency for several decades (*12*, *25*). To protect itself against oxidative stress, the lens evolved with an anaerobic biological system comprising high concentrations of glutathione (GSH) (*26*, *27*). GSH in the lens serves multiple functions, including antioxidant defense, intracellular redox homeostasis, cysteine carrier and storage, and detoxification of certain aldehydes (*27*). Lens GSH homeostasis is maintained through de novo synthesis in the lens epithelial and outer cortical layers, and GSH recycles via γ-glutamyltranspeptidase and dipeptidase (*28*, *29*) and direct uptake from the aqueous and vitreous (*30*–*32*).

While numerous studies have shown that acute or chronic depletion of GSH by chemical or genetic means is associated with cataract formation in vitro and in vivo (*33*–*35*), the role of aging in the lenticular decline in GSH levels, particularly after the age of 65, is unknown. Solving this conundrum is considered of key importance for the prevention of age-related cataract formation (*27*, *36*), as first proposed 77 years ago (*37*). Our present study has discovered an age-related truncation of the enzyme γ-glutamylcysteine ligase catalytic subunit (GCLC), a critical enzyme involved in GSH biosynthesis. This truncation impairs intracellular GSH synthesis

[1]Department of Cellular Biology and Anatomy, Medical College of Georgia at Augusta University, Augusta, GA 30912, USA. [2]Department of Pharmacology, Case Western Reserve University, Cleveland, OH 44106, USA. [3]Department of Ophthalmology, Medical College of Georgia at Augusta University, Augusta, GA 30912, USA. [4]Department of Pathology and Biochemistry, Case Western Reserve University, Cleveland, OH 44106, USA.
*Corresponding author. Email: xfan@augusta.edu
†These authors contributed equally to this work.

and contributes to diminished GSH levels in aged lenses. Blocking GCLC truncation preserves GSH levels in aged lenses and significantly delays cataract formation.

RESULTS

GCLC undergoes age-related truncation in mouse and human lenses

γ-Glutamylcysteine ligase (GCL) is a critical enzyme involved in the biosynthesis of intracellular GSH, acting as the rate-limiting step. GCL is composed of two subunits: the catalytic subunit (GCLC) and the modifier subunit (GCLM). While GCLC has the catalytic domain, its interaction with GCLM is necessary for optimal enzymatic activity (*38*). During our investigation of GCLC protein expression in aged mouse lenses, we unexpectedly observed a smaller molecular weight band, approximately 60,000 Da (referred to as G60 in this study). Intriguingly, G60 exhibited an age-related increase in mouse lenses and reached similar levels to the full-length GCLC (termed G73 in this study) in aged lenses (Fig. 1A). We also analyzed collected human lenses with an average postmortem interval of 18 hours and observed a similar age-related increase in G60 (Fig. 1B). Calculating the ratio of G60 to G73, we identified a positive age association (R^2, 0.6772) in human lenses (Fig. 1C). On the basis of age-related human lens growth and physiological behavior, we categorized lenses into four groups: below 20 years (group I) as a period of rapid growth, 21 to 40 years (group II) as the optimal performance period, 41 to 65 years (group III) as a period prone to presbyopia development, and beyond 65 years (66 to 100 years, group IV) associated with higher cataractogenesis. We observed a nearly linear relationship of G60/G73 from groups I to IV (Fig. 1D). Notably, full-length GCLC (G73) levels were also increased in aged mice and human lenses (Fig. 1, A and B). Through comparisons with Gclc knockout (KO) mouse lenses (Fig. 1E), we confirmed that this band represents a truncated form of GCLC (Fig. 1A). To examine the condition of the smaller truncated fragment with a size around 13 kDa (termed G13 in this study), we generated an antibody that specifically recognizes G13 using a mouse G13 recombinant fragment (fig. S1). With this antibody, we detected an age-related increase in the G13 fragment in mouse lenses (Fig. 1A), suggesting that the truncated G13 fragment is also stably present in the aged lens. Unfortunately, our homemade C-terminal antibody did not recognize the human G13 fragment.

To determine whether GCLC truncation occurs in tissues other than the lens as part of the aging process, we measured G60 levels by immunoblotting in 12-month-old mice. We detected the presence of G60 in the liver, lung, blood, and kidney but not in the brain, muscle, heart, and spleen (Fig. 1E). However, G60-to-G73 ratios in these tissues were much lower compared to the lens (Fig. 1E), and no age-related increase was observed (fig. S2). G60 proteoform was only detected in red blood cells and not in white blood cells (fig. S3). In addition, we did not observe GCLC truncation in the in vitro–cultured cell lines, such as retinal pigmented epithelial (RPE), human lens epithelial (FHL124 and HLEB3), human embryonic kidney (HEK) 293, and colon cancer (SW480 and DLD1) cell lines (Fig. 1F).

To examine the spatial distribution of the G60 proteoform, we isolated lens epithelium and fiber sections from both mouse (12 months) and human (45 years) lenses, revealing that G60 was specifically present in the lens fiber cells (Fig. 1, G and H).

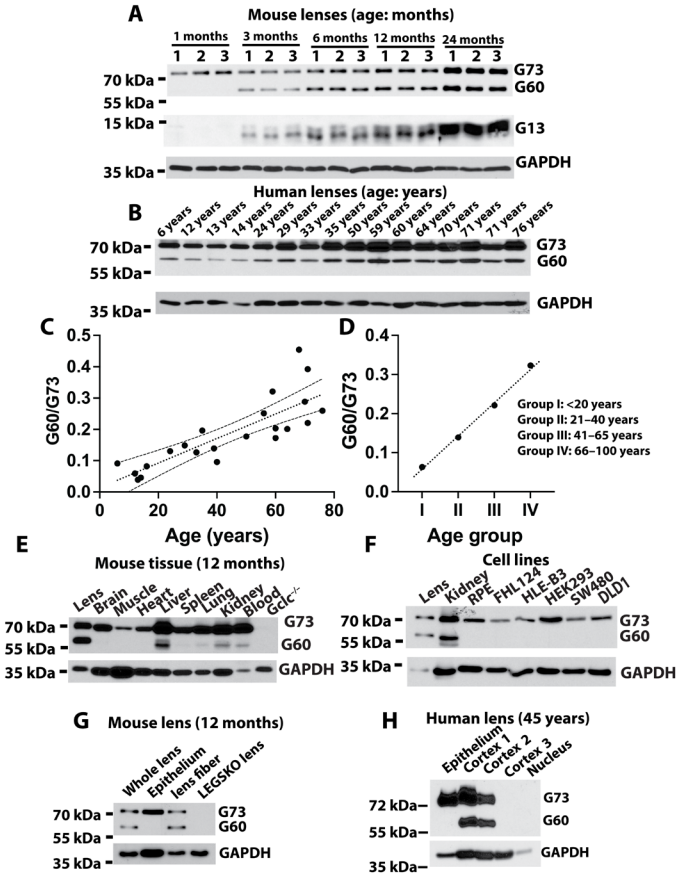

Fig. 1. Age-related increase of GCLC truncation in mouse and human lenses. Immunoblotting using specific antibodies was used to determine G73 and G60. The C-terminal fragment (G13) was also measured using an antibody recognizing the entire mouse G13 fragment. (**A**) Mouse lenses aged 1 month to 24 months were analyzed. These data represent three individual mouse lenses from each age group, and measurements were taken from a minimum of six mice in each group. (**B**) Human lenses with ages ranging from 6 to 76 years were also studied. (**C**) The relationship between the ratio of G60/G73 and age in human lenses was examined. Regression analysis with 95% confidence intervals (CI) yielded the following prediction: $y = 0.0039x + 0.0138$, $r = 0.8229$, $P < 0.0001$, $n = 22$. (**D**) The correlation between the ratio of G60/G73 and age range groups in human lenses was investigated. The regression line was found to be $y = 0.0861x + 0.0286$, $r = 0.9976$. (**E**) The occurrence of GCLC truncation in other aged mouse tissues. Blood was effectively removed through cardiac perfusion in all vascular tissues. (**F**) GCLC truncation in cultured cell lines. Note: The kidney tissue used as an additional positive control in (F) was not obtained through cardiac perfusion. Consequently, it reflects a mixture of G60 levels from both kidney and red blood cells. (**G**) The spatial distribution of G73 truncation in mouse lenses showed no detectable G60 in the lens epithelium, while notable G60 was observed in the lens fibers. (**H**) The spatial distribution of G73 truncation in human lenses indicated no detectable G60 in the human lens epithelium, while major G60 was present in the outer layer of the lens cortex, with no G60 detected in the lens nucleus. GAPDH, glyceraldehyde phosphate dehydrogenase.

GCL activity continuously declines during aging in human and mouse lenses

We further investigated the biological significance of GCLC truncation in the decline of lens GSH concentration during the aging process. To begin with, we used the liquid chromatography–mass spectrometry (LC-MS) method and observed a remarkable age-related

decrease in GCL activity in the human lens (Fig. 2A). This finding corroborated the results of a prior report that used a colorimetric-based method (*39*). The decline in GCL activity associated with age was also observed in the mouse lens. Notably, there was a significant approximately twofold decrease in GCL activity in 20-month-old lenses when compared to their 3-month-old counterparts (Fig. 2B). Furthermore, in line with expectations, we noted a concurrent age-related decrease in lens GSH levels (Fig. 2C). There was a clear correlation between lenticular GSH levels and GCL activities, as depicted in Fig. 2D. These findings strongly emphasize the pivotal role of GCL activity in maintaining lens GSH homeostasis.

To gain further insights, we conducted measurements of spatial GCL activity in both young (2-month-old) and old (20-month-old) lens epithelium and outer cortex, where cellular transcriptional and translational machinery remains active. We observed that the GCL activity in the lens epithelium remained relatively constant even at an advanced age (Fig. 2E). However, the outer cortical region of the lens exhibited a significant decrease in GCL activity as the lens aged (Fig. 2E). This decrease correlated with the spatial and temporal pattern of age-related GCLC truncation.

G60 proteoform is derived from GCLC cleavage at aspartate 499 (D499)

To investigate the nature of the G60 proteoform, we performed immunoprecipitation (IP) using a GCLC antibody specific to the N-terminal region to purify the G60 proteoform from 114 lenses of aged mice (>8 months old) (fig. S4). Mass spectrometry analysis revealed a tryptic fragment resulting from cleavage between aspartic acid 499 and glycine 500, as compared to full-length GCLC (Fig. 2, F and G). This finding strongly suggests that G60 is the result of cleavage at the D499-G500 site in the aged lens.

In 2002, Franklin *et al.* (*40*) discovered that in in vitro cell cultures, the GCLC protein could undergo cleavage during apoptosis. This cleavage was triggered by cell death receptor–mediated pathways, such as tumor necrosis factor–α (TNFα) or anti-Fas. The resulting 60-kDa truncation band was attributed to the cleavage by caspase 3 at the D499 site. Recognizing the consistent GCLC cleavage site both in vitro and in vivo, we experimented with in vitro–induced conditions. Upon treatment with TNFα/cycloheximide (CHX) or staurosporine (STS), we successfully induced GCLC truncation and G60 formation in HeLa and mouse embryonic fibroblast (MEF) cells, as shown in Fig. 2H and other figures.

To further validate the lens GCLC cleavage site observation, we conducted mutagenesis experiments using in vitro culturing models. We overexpressed wild-type (WT) GCLC, as well as D499A and D499E mutant forms, all tag-free, in Gclc KO MEF cells. After treating the cells with 500 nM STS for 4 hours, G60 production was inhibited in both the D499A and D499E mutant GCLC constructs (Fig. 2H).

Calpain, caspases 1, 3, 6, and 12, and fiber cell differentiation are not responsible for lens GCLC cleavage

The pivotal role of caspase 3 in GCLC cleavage within the in vitro cell culture system inspired us to explore whether it plays a similar role in GCLC truncation during the aging process of the lens. We conducted experiments to assess GCLC truncation in two distinct KO lens models: caspase 3 KO (6 months old, as shown in fig. S5B) and caspase 6 KO (9 months old, as shown in fig. S5C), both of which are considered executioner caspases. In addition, we examined GCLC truncation in caspase 1 KO (20 months old, as shown in fig. S5D) and caspase 12 KO (7 months old, as shown in fig. S5E) lenses, which are associated with inflammatory responses. Intriguingly, even with substantial inhibition of GCLC cleavage using pan-caspase, caspase 3, and caspase 6 inhibitors in TNFα plus CHX–treated HeLa cells (fig. S5A), we observed no significant reduction in GCLC cleavage across all tested caspase KO mouse lenses. Further investigation into the spatial expression of the two executioner caspases revealed that both caspases 3 and 6 are primarily expressed in the lens epithelium (fig. S5, F and G). These results suggest a distinct cleavage mechanism between in vivo GCLC truncation and in vitro–induced cell death cleavage, at least with regard to caspase 1, 3, 6, and 12–mediated mechanisms. It is worth noting that we did not conduct experiments involving executioner caspase 7 and other caspases.

We exclusively detected GCLC truncation within the lens fiber cells. Lens fiber cells originate from lens epithelial cells through the process of cell differentiation. Several studies suggest that non-apoptotic caspase 3 activation plays a role in the lens epithelial cell differentiation process (*41*–*44*). This suggests the plausible hypothesis that GCLC is a byproduct of lens epithelial cell differentiation. To test this hypothesis, we conducted an ex vivo lens capsular explant culture system, inducing lens capsular epithelial cell differentiation through fibroblast growth factor 2 (FGF-2) treatment (200 ng/ml). As shown in fig. S6A, 48 hours after FGF-2 treatment, we observed elongated cells in the lens capsule demonstrating fiber cell formation. Immunofluorescence staining (fig. S6B) and immunoblotting (fig. S6C) using the β crystallin antibody demonstrated a significant increase in β crystallin expression in the FGF-2–induced capsules compared to the untreated control capsules. However, we did not observe any GCLC cleavage in the FGF-2–treated or nontreated capsules (fig. S6C).

Calpains, which are calcium-dependent cysteine proteases, have been identified as responsible for the proteolytic cleavage of lens crystallin and the formation of cataracts (*45*–*47*). This raises the question of whether calpains may also play a role in the production of age-related G60. To investigate this, we conducted an in vitro calpain proteolytic digestion of recombinant GCLC protein using native calpain-1. To ensure that the digestion conditions activated calpain, we optimized the conditions using a fluorogenic peptide substrate and further validated the results with a calpain inhibitor (fig. S7A). As illustrated in fig. S7B, while calpain proteolytic cleavage was able to partially digest G73, it was unable to generate G60.

G60 proteoform significantly impairs GCLM binding and almost completely abolishes enzymatic activity

To investigate the structural changes caused by GCLC truncation, we used AlphaFold to model human intact GCLC, truncated GCLC (G60 and G13), and their interactions with GCLM. AlphaFold successfully predicted the formation of the GCLC-GCLM heterodimer. In the visualization (Fig. 3A), GCLM is represented in light red color, while GCLC is depicted in blue (G60) and rainbow (G13). The C-terminal G13 motif, particularly two helical structures, is predicted to be critical for GCLM binding. To confirm that the G13 is indeed a crucial motif for the heterodimer formation between GCLC and GCLM, we overexpressed Flag-tagged G73 and G60 in HeLa cells, pull down interacting proteins by a flag-tag antibody. The results showed that GCLM was not detectable in G60 overexpressed cells

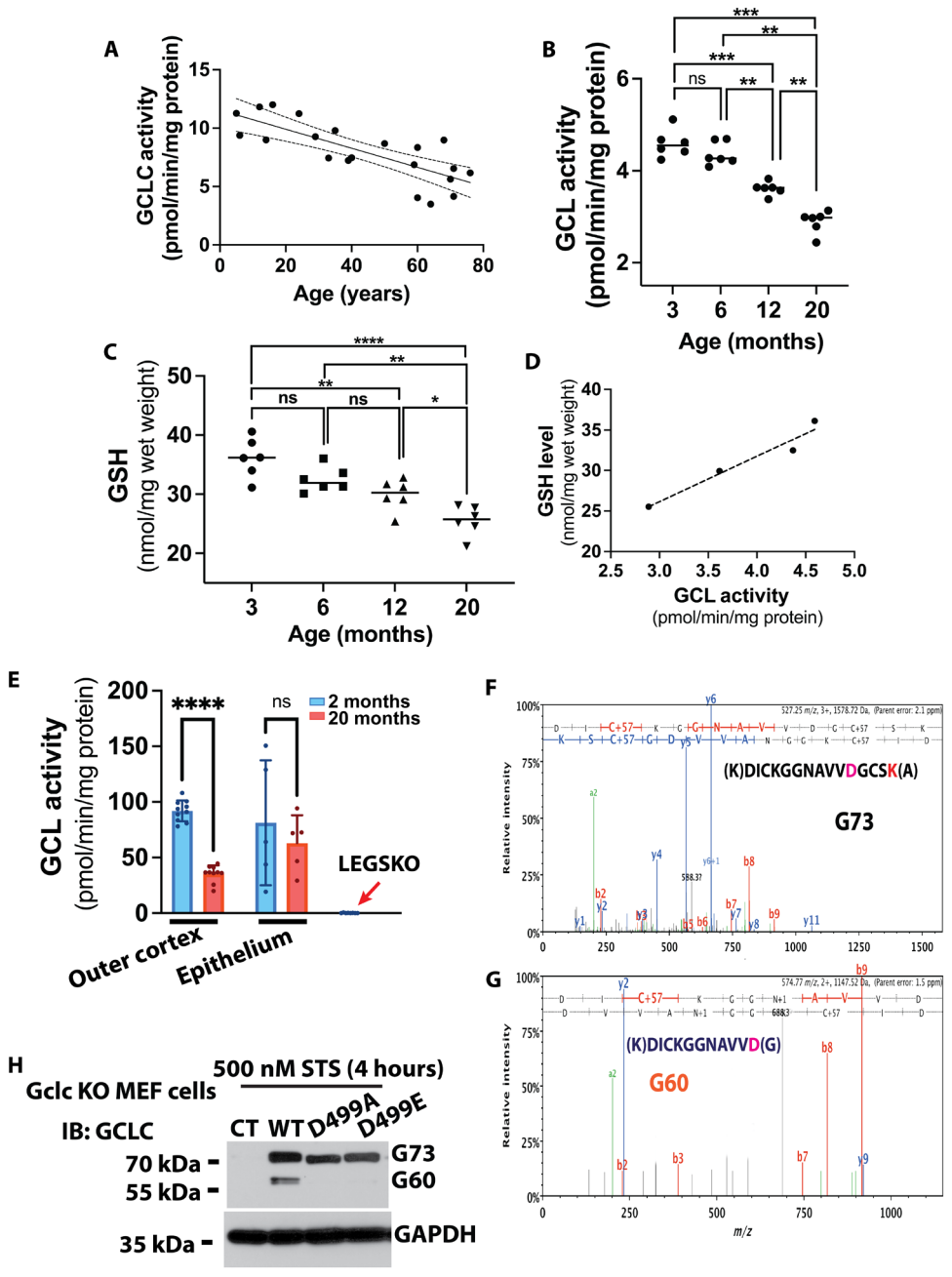

Fig. 2. Aspartate 499 GCLC cleavage in cortical fibers correlates with age-related decline of GCL activity. (**A**) An age-related decline in GCL activity was observed in human lenses. Regression analysis with 95% CI yielded the following prediction: $y = -0.08151x + 11.54$, $r = 0.7787$, $P < 0.0001$, $n = 21$. (**B**) An age-related decline in GCL activity was observed in mouse lenses. (**C**) An age-related decline in lens GSH was observed in mouse lenses. (**D**) The correlation between lens GSH level and GCL activity was investigated. The regression line was found to be $y = 5.606x + 9.325$, $r = 0.9741$. (**E**) Significantly decreased GCL activity was found in the lens outer cortex but not epithelium when comparing 20-month-old mouse lenses to 2-month-old mouse lenses. (**F** and **G**) G73 and G60 were immunoprecipitated under denaturing conditions using a GCLC antibody recognizing the N-terminal region of protein GCLC. Mass spectrometry analysis revealed the detection of the theoretic tryptic peptide of the full-length GCLC, DICKGGNAVVDGCSK (F), and the cleavage peptide DICKGGNAVVD (G). (**H**) Tag-free GCLC was expressed in Gclc KO MEF cells using retroviral particle infection. Following induction of MEF cell death with 500 nM STS for 6 hours, G73 and G60 were determined by immunoblot (IB). Consistent with the findings, D499A and D499E mutations prevented G73 cleavage. CT, control cells without viral infection. (E) Results were expressed as mean ± SD and were analyzed using Student's *t* test. (B and C) Results were expressed as mean ± SD and were analyzed using one-way analysis of variance (ANOVA) with Tukey's multiple comparisons test. Only $P < 0.05$ is considered significant. *$P < 0.05$, **$P < 0.01$, ***$P < 0.001$, and ****$P < 0.0001$. ns, not significant; *m/z*, mass/charge ratio.

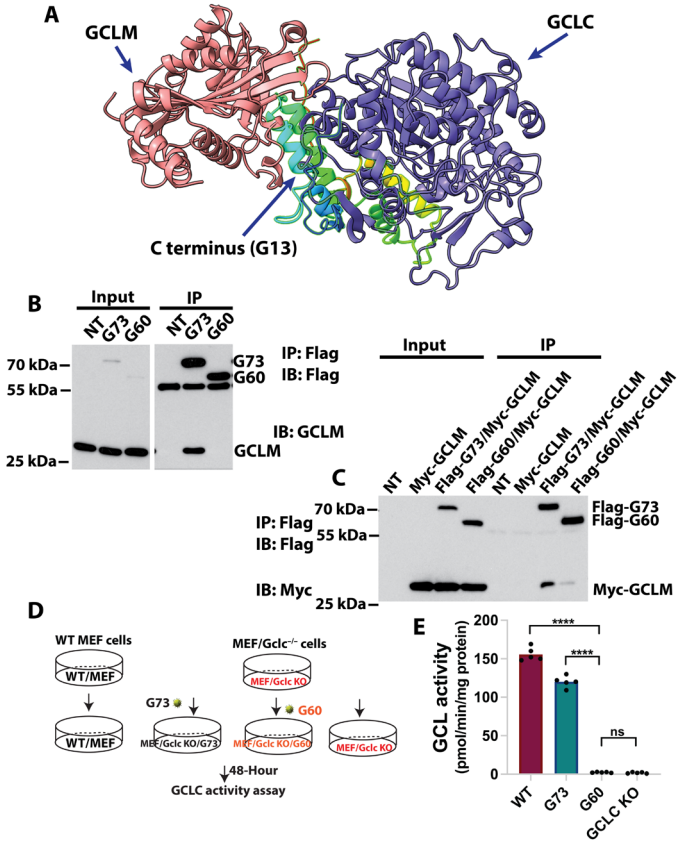

Fig. 3. GCLC cleavage fragment G60 abolishes GCLM binding and enzymatic activity. (**A**) AlphaFold-multimer 2 predicted the protein complex, and the C-terminal motif was found to be crucial for GCL holoenzyme formation by GCLC and GCLM. (**B**) Co-IP in HeLa cell culture revealed that overexpressing flag-tag G73 could pull down GCLM, while no detectable GCLM was found in G60 overexpressed cells. (**C**) In HeLa cell culture, substantial levels of GCLM were pulled down when both flag-tag G73 and Myc-tag GCLM were overexpressed. Conversely, only a weak GCLM band was detected in both flag-tag G60 and Myc-tag GCLM overexpressed HeLa cells. (**D**) G60 activity was assessed by expressing G73 and G60 in Gclc KO MEF cells. The cell lysate, collected 48 hours after viral particle infection, was used for GCL activity analysis. WT MEF cells were used as a control. (**E**) The results of GCL activity from (D) demonstrate that G60 nearly completely abolishes its enzymatic activity. One-way ANOVA with Tukey's honest post hoc analysis was used to compare between groups, and only $P < 0.05$ is considered significant. (****$P < 0.0001$).

when compared to G73 overexpression (Fig. 3B). We only observed a weak G60 and GCLM binding when both G60 and GCLM were overexpressed together (Fig. 3C). These findings indicate that G60 has a significantly weaker binding affinity with GCLM and cannot compete with full-length GCLC in heterodimer enzyme formation. Consequently, the disruption of heterodimer formation after GCLC truncation is likely to have an impact on enzymatic activity.

To assess the enzymatic activity of G60 compared to G73, we conducted measurements using WT and Gclc KO MEF cell culture systems (Fig. 3D). As demonstrated in Fig. 3E, G60 almost completely abolished GCLC catalytic activity, highlighting the importance of the C-terminal region, particularly the G13 motif, in maintaining GCLC's functional enzymatic activity.

G60 competes with GCLM binding in the presence of the G13 fragment

By cleaving GCLC at aspartate 499, two truncated fragments are produced: the N-terminal fragment G60 and a C-terminal fragment G13. The presence of both truncated fragments prompted us to investigate whether G60 can bind GCLM in conjunction with G13.

To explore this, we developed an intracellular ectopic protein expression system in GCLC KO HeLa cells. These approaches not only minimized interference from endogenous GCLC but also avoided adding methionine to facilitate G13 overexpression. The ectopic protein expression system used a ubiquitin-fusion approach, resulting in self-cleavage and the production of an exact G13 fragment as observed in vivo (fig. S8). When flag-tagged G73 or G60 was coexpressed with G13 in the GCLC KO HeLa cells, we observed G13 pulldown with the flag-tag antibody only in the presence of G60 and G13 coexpression (Fig. 4A). No binding was observed between G73 and G13, indicating that G60 still interacts with G13. Subsequently, we investigated the potential binding of G60 to GCLM in coordination with G13. Using the same GCLC KO HeLa cell system, we coexpressed G13, flag-tagged G73, and G60. IP using the flag-tag antibody yielded consistent levels of GCLM between cells cooverexpressing G73 and those cooverexpressing G60 plus G13, implying a similar binding propensity of G60 plus G13 to GCLM (Fig. 4, B and C). In addition, when we coexpressed tag-free versions of G73, G60, G13, or G60 plus G13 alongside flag-tagged G73 in the GCLC KO HeLa cells, both tag-free G73 and combination of G60 and G13 demonstrated equal binding competitiveness with flag-tagged G73 for GCLM (Fig. 4D). This was not observed when G60 or G13 was expressed individually (Fig. 4D). These outcomes compellingly show that the combination of G60 and G13 has the same binding competition as G73 when it comes to GCLM.

Corroborating our findings, AlphaFold's predictions also discerned the two fragments, G60 and G13, in tandem with the formation of a GCLM complex. These data suggest that G13 may act as a bridge connecting GCLM and G60 (Fig. 4E).

The equivalent binding affinity of G60 plus G13 to GCLM raises critical questions regarding enzymatic activity. To investigate this further, we gradually overexpressed tag-free G73, G60, and G13 in GCLC KO HeLa cells and measured both enzymatic activity and intracellular synthesis of the substrate GSH. Despite exhibiting similar GCLM binding affinity, G60 plus G13 coexpression displayed significantly lower enzymatic activity (Fig. 5, A and B) and intracellular GSH synthesis (Fig. 5, C and D) compared to G73 alone. We observed rapid degradation of G13 when it was overexpressed alone, but coexpression with G60 significantly prolonged the presence of intracellular G13 (Fig. 5, E and F). These findings suggest that the formation of the G60 and G13 heterodimer may stabilize G13, protecting it from degradation.

D499E knock-in mouse inhibits GCLC truncation and maintains lens GSH levels

If GCLC truncation does indeed impair intracellular GSH biosynthesis during lens aging, then preventing GCLC fragmentation could potentially help maintain GSH levels in the aged lens. To explore this possibility, we decided to create a knock-in (KI) mouse model carrying mutations that could effectively block GCLC truncation, and the optimal mutation site for this purpose was identified as aspartate 499. We conducted an in vitro cell apoptosis culture assay to evaluate the efficacy of D499E and D499A mutations in

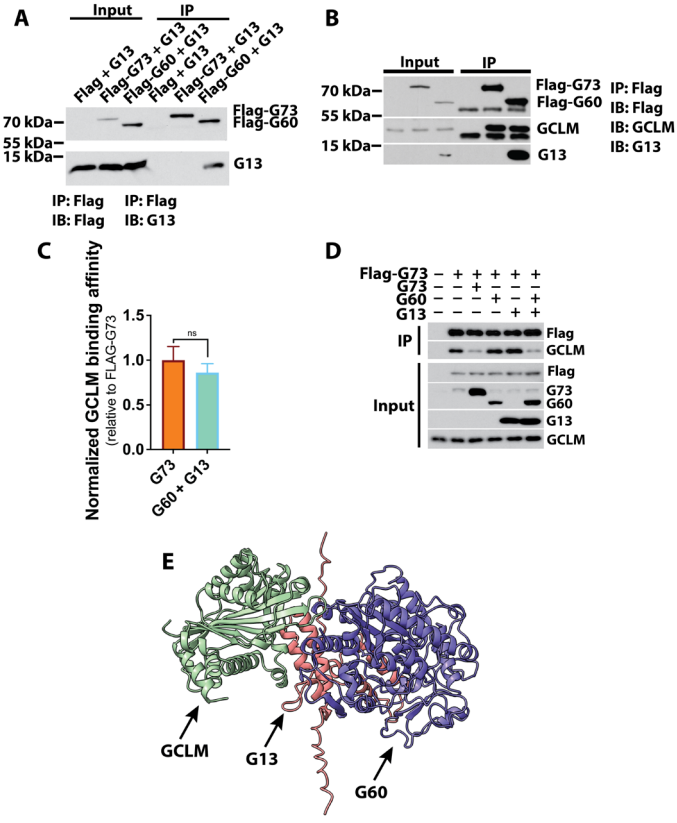

Fig. 4. G60 and G13 coordinately bind GCLM, competing with G73. (**A**) G60, but not G73, interacts with G13. Either the flag vector alone, flag-tag G73, or flag-tag G60 was expressed in HeLa cells with or without coexpression of G13. Only flag-tag G60 was able to pull down G13 in G60 and G13 coexpressed cells, demonstrating that G60 could still bind the G13 fragment. (**B**) The IP study demonstrated that coexpressing G60 and G13 could pull down an equal amount of GCLM compared to cells expressing G73. Flag-tag G60 was coexpressed with G13 and then compared with cells expressing flag-G73. The flag antibody IP was able to pull down an equal amount of endogenous GCLM. (**C**) Quantitative results from three repeats ($n = 3$) of (B) experiment. (**D**) G73 and the combination of G60 and G13 equally competed with flag tagged G73 for GCLM binding. In GCLC KO HeLa cells, flag tagged G73 was cooverexpressed with tag free G73, G60, G13, and G60 plus G13. GCLM was determined from IP product by flag tag antibody. (**E**) AlphaFold successfully predicted that G13 could act as a patch between GCLM and G60. All experiments in this figure used a transient ectopic expression system. One-way ANOVA with Tukey's honest post hoc analysis was used to compare between groups, and only $P < 0.05$ is considered significant. (ns, not significant).

blocking GCLC truncation. As depicted in Fig. 6A, both D499A and D499E mutations were successful in preventing GCLC truncation. Notably, in the case of the D499E mutant GCLC, partial truncation was observed after prolonged exposure (Fig. 6A). Furthermore, we assessed the GCL enzymatic activity of these mutations in comparison to the WT and found that D499E maintained a similar GCL enzymatic activity as compared to WT, while D499A significantly compromised GCL enzymatic activity (Fig. 6B). Considering the similar binding affinity with GCLM and enzymatic activity relative to WT GCLC for D499E (Fig. 6, B and C), we opted for the D499E-KI model for our subsequent in vivo animal studies to avoid major charge shifts. D499E-KI mouse model was created by CRISPR-Cas9 technology with only a single mutation (GAC > GAA) to convert aspartate to glutamate.

Considering that caspases have the potential to cleave GCLC and given the reported important role of cell apoptosis in lens development (*48*–*50*), we measured lens cell apoptosis using terminal deoxynucleotidyl transferase–mediated deoxyuridine triphosphate nick end labeling (TUNEL) assay at key developmental time points, specifically embryonic day 13.5 (E13.5), E15.5, and E18.5, in both WT and D499E-KI homozygous embryos. Our observations revealed the presence of TUNEL-positive signals at E18.5, primarily localized within the active cell differentiation zone (fig. S9, A to F). However, we did not detect reliable TUNEL-positive signals at E13.5 and E15.5. In our analysis, we found no significant differences between WT and D499E-KI mice in terms of lens cell apoptosis (fig. S9G). Furthermore, conducting thorough comparative studies of lens morphology at E13.5, E15.5, E18.5, and postnatal day 0 (P0) did not yield any discernible distinctions between WT and D499E-KI mice (fig. S10). These collective findings strongly suggest that the aspartate-to-glutamate mutation at residue 499 does not exert any influence on lens cell apoptosis during lens development, nor does it affect overall lens development.

If GCLC truncation indeed impairs intracellular GSH biosynthesis during lens aging, then blocking GCLC cleavage could maintain GSH levels in the aged lens. When we measured 14- and 20-month-old mouse lenses, GCLC truncation was significantly suppressed in the D499E-KI mouse lenses (Fig. 6, D and E). Unexpectedly, although we expected milder protein truncation in the in vivo lens, a substantial amount of GCLC truncation was still detected in aged D499E-KI mouse lenses. Nevertheless, suppressing GCLC truncation led to a significant increase in aged lens GSH levels (Fig. 6F).

To assess the impact on age-related cataract formation, we screened 94 20-month-old WT C57BL/6 mice (54 males and 40 females) and 100 D499E-KI mice (54 males and 46 females) using slit lamp examination. Cataracts were classified into three distinct grades based on their size and density: grade I (no cataracts), grade II (mild cataracts), and grade III (severe cataracts). In Fig. 7 (A to C), we present a comprehensive view of the degree of cataract severity using full eye images captured by slit lamp examination. Figure 7 (D to F) depicts the slit images for further clarity, while Fig. 7 (G to I) provides a visual representation of dissected lens dark-field images. In addition, Fig. 7 (J to L) presents a grid view of these lenses at their respective grades. Both grade II and grade III lenses exhibit noticeable aggregation in the central anterior region of the lens. To pinpoint the exact location of these aggregates, we conducted isolation of lens fibers and capsules. As depicted in fig. S11, our observations revealed that aggregates were exclusively present in the outer cortical layer of grade II lenses, with no opacification detected in the lens capsules. In lenses with severe cataracts (grade III), we observed intense aggregation and opacification in the outer cortical layer, coupled with minor aggregation in the lens capsule and epithelium. These findings collectively suggest that the initiation of lens aggregation and opacification predominantly occurs within the fiber layer, and severe fiber aggregation can subsequently lead to opacification in the lens capsule. In addition, these findings closely parallel the GCLC truncation, which primarily inhibits GSH synthesis in the outer cortical layer of the lens.

By 20 months of age, approximately 19.9% of WT mouse lenses were cataract-free, while about 49.5% of KI mouse lenses showed no cataracts—a 2.5-fold increase in cataract-free lenses when GCLC truncation was suppressed (Fig. 7M). Moreover, both mild and severe cataracts (grades II and III) were reduced in D499E-KI

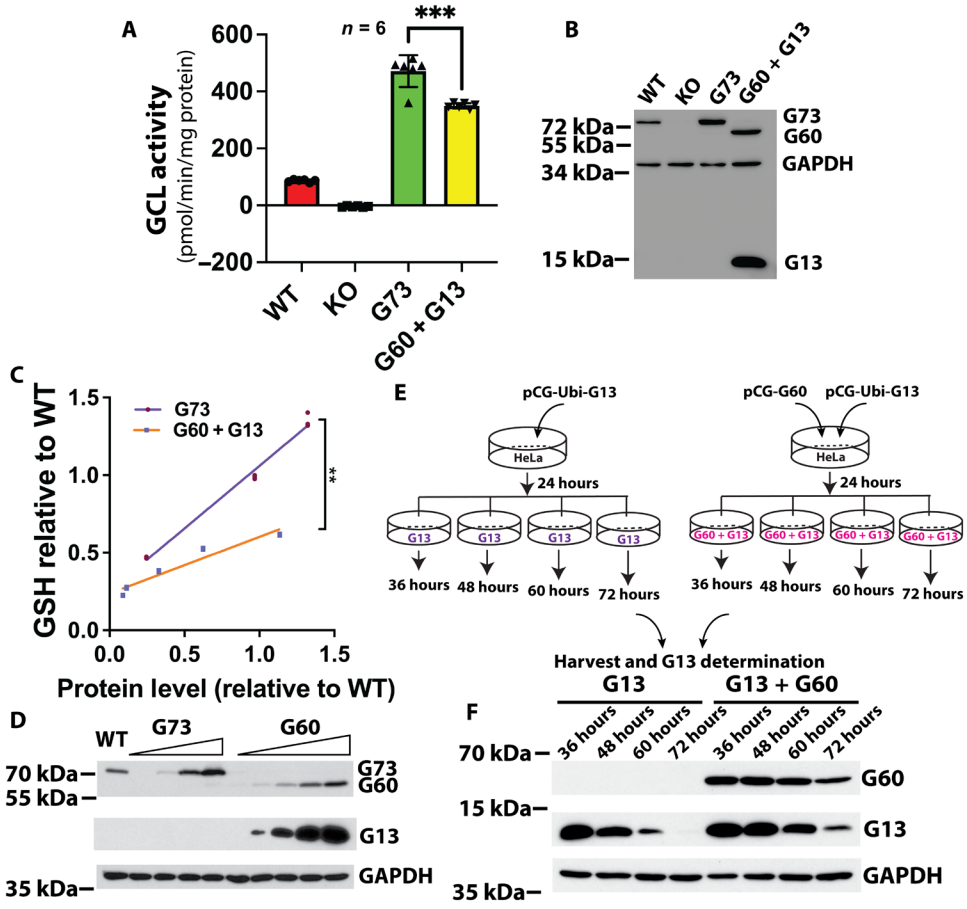

Fig. 5. G60, G13, and GCLM complex significantly impair GCL enzymatic activity. (**A** and **B**) GCL activity was significantly decreased in GCL holoenzyme assembled by G60, G13, and GCLM compared to G73 and GCLM. GCLC KO HeLa cells were used in the GCL activity assay. Approximately equal amounts of G73 and G60 (coexpressed with G13) were achieved (B), and the GCL activity was significantly lower in G60/G13-expressed cells than in G73-expressed cells (A). (**C** and **D**) Significantly lower levels of GSH were produced in G60/G13 coexpressed cells than in G73-expressed cells. In GCLC KO HeLa cells, a gradual increase in the expression of either G73 or G60/G13 was conducted (D). G60/G13 coexpressed cells generated a remarkably smaller amount of GSH than G73-expressed cells (C). Linear regression for G73: $y = 0.8060x + 0.2536$, $r = 0.9957$; for G60/G13: $y = 0.3661x + 0.2364$, $r = 0.9648$. The P value between G73 and G60/G13 = 0.0081. (**E** and **F**) G60 can stabilize G13. In GCLC KO HeLa cells, either G13 or G13 plus G60 overexpression was conducted by transient transfection. Cells were then split into four equal dishes and cultured from 36 to 72 hours. The G13 levels at each time point were determined by immunoblotting assay. G60 coexpression significantly prevented G13 degradation. All experiments in this figure used a transient ectopic expression system. One-way ANOVA with Tukey's honest post hoc analysis was used to compare between groups, and only $P < 0.05$ is considered significant. (**$P < 0.01$ and ***$P < 0.001$).

compared to WT lenses (Fig. 7M). We conducted a chi-square test to compare the rate of cataract formation and found that D499E-KI mice exhibited a significant reduction ($P < 0.0001$) in cataract formation compared to WT mice. Furthermore, measurements of both cataract size and density, as depicted in Fig. 7 (N and O), also demonstrated a significant reduction ($P < 0.0001$) in cataract size and density in D499E-KI mice.

There was no significant difference in the rate of cataract formation between male and female mice at 20 months of age. It is important to note that our D499E-KI mice were maintained on the C57BL/6J genetic background, while the WT mice used as controls in this study were on the C57BL/6JN genetic background. This minor discrepancy in genetic background raised concerns regarding whether C57BL/6JN mice might exhibit a higher rate of cataract formation compared to C57BL/6J mice. To address this concern and provide clarification, we conducted a thorough screening of 20 mice (comprising 10 males and 10 females) on the C57BL/6J genetic background to compare their cataract formation rates with those of C57BL/6JN mice. As depicted in fig. S12, both strains exhibited nearly identical rates of cataract formation. These data validation reinforces and supports our research findings.

DISCUSSION

Several factors contribute to the age-related decline of lens GSH. The primary and most crucial contributor is impaired GSH biosynthesis enzyme activity. Our present study, in line with previous research (*39*), reveals a profound decline in GCL activity in the human lens. However, the underlying mechanisms responsible for this impairment have yet to be fully understood. Our discovery of an age-related GCLC truncation provides a compelling explanation for the profound decline of lens GSH during the aging process. Conversely,

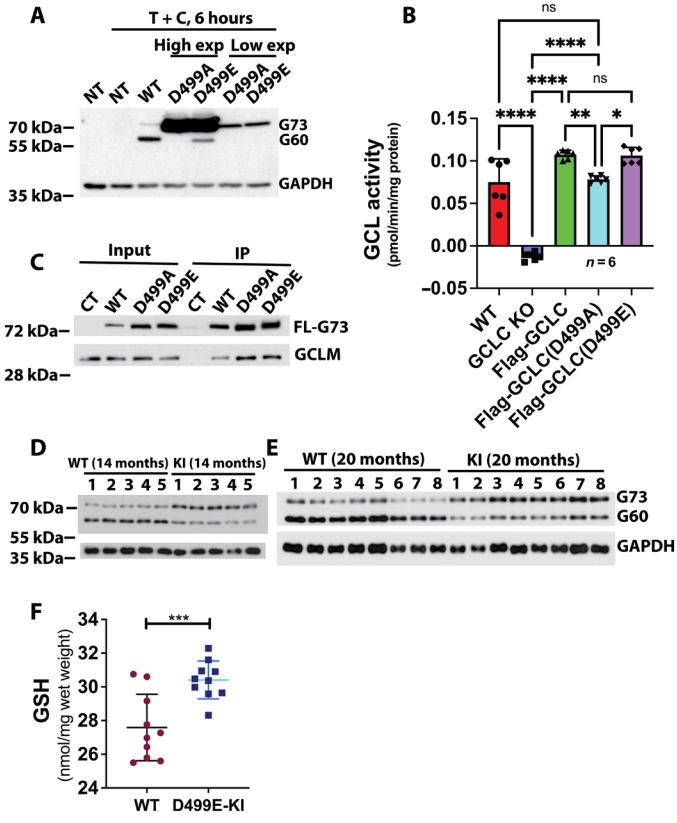

Fig. 6. D499E-KI mice alleviates GCLC cleavage and maintains lens GSH levels in aged mice. (**A**) On the basis of in vitro apoptotic cell culture model, D499E largely blocks G73 cleavage, while D499A almost completely blocks G73 cleavage. In vitro HeLa cell apoptosis induction conditions: Cell death was induced by TNFα (30 ng/ml) and CHX (10 μg/ml) for 6 hours. G73 and G60 were determined by immunoblotting assay. Short (low exp) and long (high exp) time exposure was used to detect G60 formation. A weak G60 band was still detectable in D499E mutant G73-expressed cells. NT indicates no transfected cells. (**B**) D499E maintained a similar activity to G73, while D499A still maintained a high enzymatic activity but significantly less than G73. (**C**) Both D499A and D499E mutations maintain complex formation between GCLM and GCLC. Flag-tagged G73 with and without mutations were overexpressed in GCLC KO HeLa cells, and GCLM was measured in the IP products from flag-tag antibody pull-down. (**D** and **E**) GCLC truncation was significantly suppressed in both 14- and 20-month-old D499E-KI mouse lenses compared to WT. (**F**) GSH level was largely preserved in aged mice compared to age-matched WT lenses at 14 months old. Unpaired *t* test was used in (F) data analysis, one-way ANOVA with Tukey's honest post hoc analysis was used to compare between groups in (B), and only $P < 0.05$ is considered significant. (*$P < 0.05$, **$P < 0.01$, ***$P < 0.001$, and ****$P < 0.0001$). TNFα plus CHX, T + C.

lens GSH levels are restored, and cataract formation is remarkably delayed if we block the GCLC truncation.

GCL serves as the rate-limiting enzyme in GSH biosynthesis (*51*). GCL is a holoenzyme composed of a 73-kDa catalytic subunit (GCLC) and a 28-kDa modifier subunit (GCLM). While GCLC has catalytic activity, GCLM lacks enzymatic function but plays a crucial role in GSH biosynthesis intracellularly by significantly reducing the K_m and increasing K_{cat} of GCLC when interacting with its substrate, glutamate (*38*). Therefore, GCLM is essential for the successful production of GSH. Notably, GCLM is less abundant compared to GCLC, making it a vital factor in the formation of the GCL holoenzyme (*38*, *52*). This importance is further confirmed by studies involving GCLM KO mice, where a reduction of more than 70% in GSH levels was observed in mouse tissues (*53*). Historically, research pinpointed that GCLC protein can be cleaved in in vitro–cultured cells. This cleavage can be incited either through cell death receptor–mediated pathways or when subjected to UV irradiation or transforming growth factor–β challenges (*40*, *54*, *55*). Until now, studies have only found GCLC truncation during in vitro cell culture when substantial apoptosis was induced. However, our present study has revealed that GCLC cleavage occurs in vivo, particularly in the lens fiber cells, in an age-related manner. Our study demonstrated that the two cleavage fragments compete with full-length GCLC for GCLM binding, resulting in a significant impairment of enzymatic activity when compared to the GCL holoenzyme formed by the full-length GCLC and GCLM (Fig. 8).

The intracellular GSH levels significantly decreased in the in vitro cytotoxin-mediated apoptotic cells associated with GCLC cleavage (*40*). Several reports stated that GSH depletion was because of elevated cellular GSH efflux since several reports have shown increased GSH efflux in cells triggered by the death receptor pathway. While GSH efflux indeed contributes to intracellular GSH depletion in death receptor–mediated cell apoptosis (*56*, *57*), we speculate that impaired GSH de novo synthesis plays a crucial role in cellular GSH homeostasis. Regarding in vivo conditions, particularly during the lens aging process, death receptor–mediated cell death has not been reported. Our present study indicates that impaired GCL activity resulting from GCLC truncation plays a critical role in the profound reduction of lens GSH content. It is worth noting that a study involving the chemotherapeutic drug etoposide-treated myeloblastic leukemia cells did observe GCLC cleavage (*58*), but there was no significant decrease in GCL activity. Another study using UV-B–irradiated human keratinocytes observed GCLC cleavage and a trend of decreased GCL activity, but the activity did not reach statistical significance. These findings were derived from cells undergoing cell death due to harsh stimulation (*54*), and the total protein levels for normalization may significantly differ.

In our study, we used GCLC KO cells to precisely quantify G73, G60, and G13 expression levels. In addition, we used a more accurate LC-MS method to measure GCL activity. These approaches should better reflect in vivo and physiological conditions. The evidence from D499E-KI mice, which maintained a higher level of GSH in the aged lens compared to WT mice, strongly supports our hypothesis. Notably, we still observed substantial G73 truncation in the lenses of D499E-KI mice. The primary reason for choosing the aspartate to glutamate mutation was their similar charges, ensuring that it would not significantly affect GCL enzymatic activity. However, it appears that the glutamate residue at position 499 is a much weaker substrate for the protease but could not completely block the cleavage. Even under caspase 3–mediated cleavage, we observed partial G73 cleavage in the apoptotic-induced in vitro cell culture model. The aspartate to alanine mutation had a much better prevention in blocking GCLC cleavage. However, the D > A mutation seems to negatively affect GCL activity. Future studies are needed to identify a suitable amino acid residue that can not only maintain GCL enzymatic activity but also completely block GCLC cleavage.

Our initial investigations involved in silico analysis, which highlighted the VVDG motif as a potential caspase substrate, particularly caspase 3. Furthermore, our in vitro assays demonstrated that pancaspase, caspase 3, and caspase 6 inhibitors could nearly completely

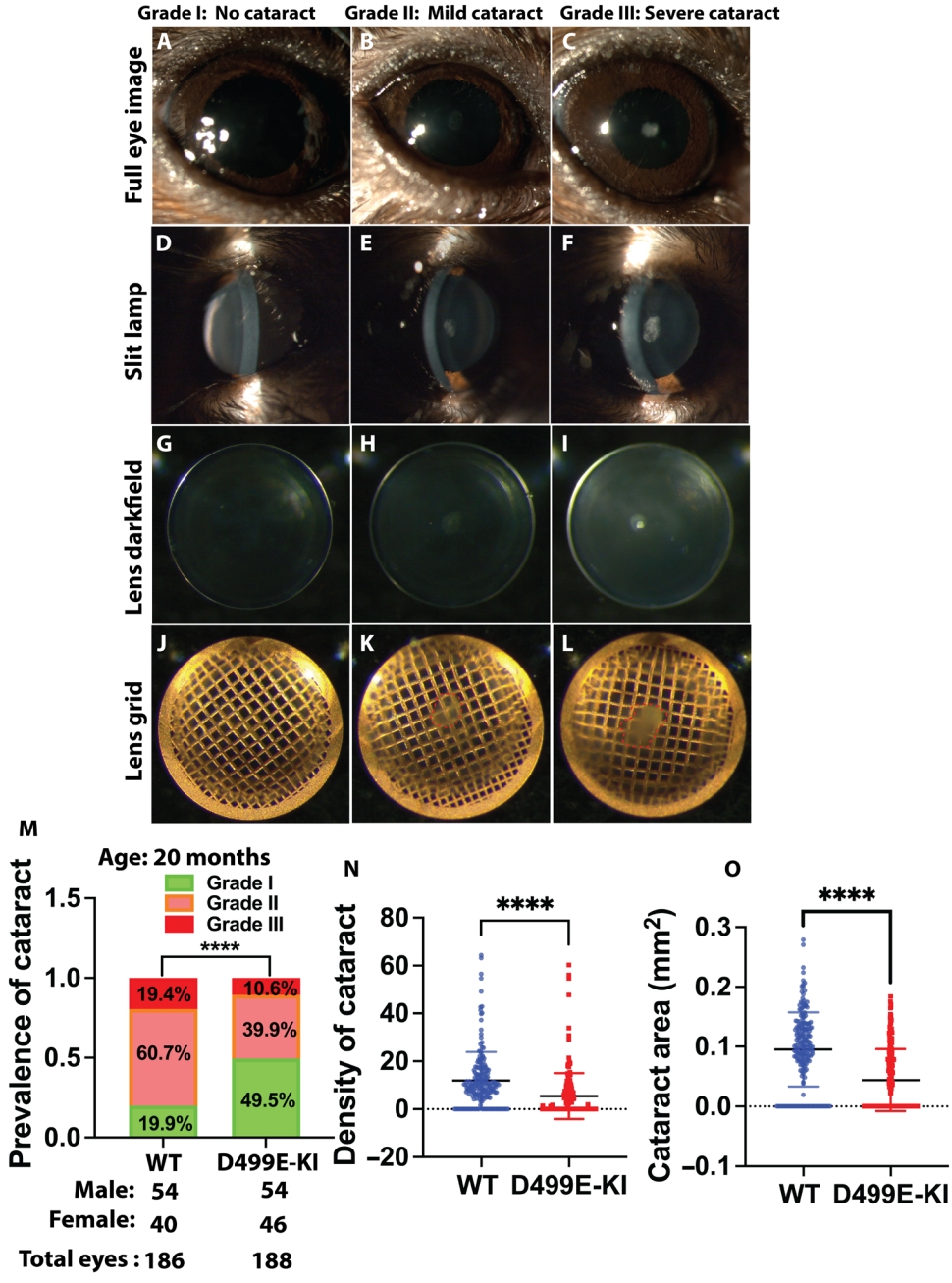

Fig. 7. D499E-KI mice significantly delay cataract formation. Twenty-month-old WT and D499E-KI mice were screened for lens opacity. Mice with corneal opacity were excluded from the study. A total of 94 WT mice (186 eyes) and 100 D499E-KI mice (188 eyes) were screened using a slit lamp. The lens opacity was categorized into three grades: grade I (no cataract), grade II (mild cataract), and grade III (severe cataract). (**A** to **C**) The full eye image exhibits varying degrees of opacity. Slit lamp settings: length, 14 mm; width, 20 mm; brightness, maximum. (**D** to **F**) Slit lamp slit images illustrate the extent of cataract severity. Slit lamp settings: length, 10 mm; width, 0.2 mm; brightness, maximum. (**G** to **I**) Lens dark-field images show opacity in the center of the anterior side. (**J** to **L**) Lens grid images depict both the opacity and the severity of cataracts, with the anterior side facing the grid. (**M**) At 20 months of age, roughly half of the D499E-KI mice remained cataract-free, contrasting with only about 20% of WT mice. Severe cataracts were observed in approximately 10% of D499E-KI mice at this age, in contrast to approximately 20% of WT mice. A chi-square test was used to compare the WT and D499E-KI groups. (**N**) Distribution of cataract density. A Mann-Whitney test was used to compare the WT and D499E-KI groups. (**O**) Distribution of cataract area. A Mann-Whitney test was used to compare the WT and D499E-KI groups. Only $P < 0.05$ is considered significant. (****$P < 0.0001$).

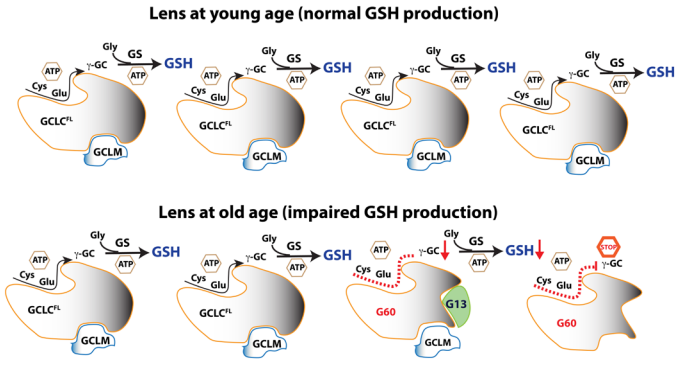

Fig. 8. Model of the role of GCLC truncation in lens GSH homeostasis during aging. In the lens at a young age, minimal GCLC cleavage occurs, leading to normal GSH biosynthesis and maintenance of GSH concentration. However, at older ages, GCLC truncation fragments compete with full-length GCLC for GCLM complex formation, resulting in impaired intracellular GSH synthesis and reduced lens GSH concentration. This age-related GCLC truncation may contribute to the decline in lens function and the development of age-related lens disorders.

block GCLC truncation in a rigorous apoptotic-induced cell culture system. However, when we conducted measurements on caspase 3 KO mice, we did not observe any prevention of GCLC truncation. Subsequently, we expanded our study to include caspase 1, 12, and 6 KO mice and found very similar results. An important discovery was that we mapped the spatial expression of key executioner caspases 3 and 6, primarily finding their expression in the lens epithelium. This observation may explain why caspases 3 and 6 are unlikely to be responsible, as GCLC truncation was only detected in the lens fibers. Our further study also excluded calpain as one of the mechanisms in age-related GCLC truncation. The mechanism of GCLC cleavage in the lens during aging remains to be elucidated.

The level of GSH in the lens decreases with age, especially in the lens nucleus, and this is widely believed to be a key factor contributing to age-related nuclear cataract formation (*24*, *36*, *59*). Apart from the notable impairment of GCL activity, there are other mechanisms that also contribute to age-related decline of GSH in the lens. Disruption of lens GSH homeostasis is influenced by factors such as decreased sources of extralenticular GSH or its constituent amino acids due to aging changes in the ciliary body, including sclerosis and reduced vascularization in the ciliary body processes (*60*, *61*). Furthermore, the age-related increase in lens stiffness and barrier formation (*62*–*66*) is associated with a decline in GSH diffusion into the inner layer of the lens. This decrease in GSH diffusion has been considered one of the mechanisms involved in age-related nuclear cataract formation. However, the precise mechanism of barrier formation is not yet fully understood. It is suggested that increased crosslinking between cytoskeletal, membrane proteins and lipids, and crystallins may contribute to the formation of this barrier. Oxidative stress-induced protein crosslinks and remodeling of membrane lipids have been identified as crucial contributors during the aging process, including protein disulfides (*67*), glycation (*15*), ascorbylation (*68*), and lipoxidation (*69*). The truncation of GCLC occurs around the mid-20s, just before the appearance of the lens barrier, which usually occurs around the 30s (*62*). This raises the question of whether the decreasing lens GSH and barrier formation are causally related or if they fall into a "chicken or the egg" causality dilemma. It is possible that the impairment of GSH biosynthesis and the decline in GSH levels early on might at least accelerate the barrier formation. In addition, impaired GSH regeneration in the aging lens further contributes to the GSH decline. GSH typically works in conjunction with GSH peroxidase, GSH reductase (GR), and glutaredoxin to form a "GSH antioxidant network." The age-related dysfunction of these redox enzymes (*70*, *71*) can hinder GSH regeneration. This is evidenced by the elevated protein-S-S-GSH mixed disulfides in the aged human lens, which have been extensively documented in previous research (*59*, *72*, *73*). In contrast, our study provides clear evidence that cataract formation can be significantly delayed by restoring lens GSH levels in aged mice. Our findings lead us to believe that preventing the cleavage of the key enzyme GCLC during lens aging may become an effective approach to restoring lens GSH levels and delaying the onset of cataract.

In conclusion, our study represents a groundbreaking discovery, identifying an age-related truncation of the GSH biosynthesis enzyme GCLC. This cleavage does not lead to a decrease in GCL holoenzyme complex formation, but it does significantly impair GCL enzymatic activity. By generating KI mice without GCLC cleavage, we demonstrated that blocking GCLC cleavage successfully maintained lens GSH levels even in older mice, and it significantly delayed age-related cataract formation. These findings open up a crucial path for developing a therapeutic approach to delay age-related cataractogenesis, potentially offering strategies to mitigate the impact of cataracts associated with aging.

METHODS

Reagents

All chemicals used were of analytical reagent grade. Milli-Q water was used for the preparation of standards and reagents. STS (A8192) was purchased from ApexBio (Boston, MA). TNFα (T7924), CHX (C1988), L-glutamic acid (G1251), L-2-aminobutyric acid (A1879), benzylamine (B5136), pyruvate kinase (10109045001), phosphoenolpyruvate (10108294001), calpain-1 (208713), calpain inhibitor III (208722), calpain substrate III fluorogenic (208771), In Situ Cell Death Detection kit TMR red (12156792910), FGF-2 (SRP4037), and adenosine triphosphate (ATP; A1852) were purchased from Millipore Sigma (St. Louis, MO). γ-Glutamylaminobutyric acid (B095384) was purchased from BenchChem (Pasadena, CA). All other chemicals were obtained from Sigma-Aldrich and Thermo Fisher Scientific.

Human donor eye tissue collection

Normal human eye globe span of 5 to 76 years old was obtained from the Georgia Eye Bank with an average postmortem time of 18 hours. The lens was then dissected and immediately processed for individual assays as described.

Animal

All animal experiments were conducted in strict adherence to the approved protocols by the Augusta University Animal Care and Use Committee, following the Association for Research in Vision and Ophthalmology guidelines for the ethical use of animals in Ophthalmic and Vision Research. The animals were housed in conditions with diurnal lighting and provided unrestricted access to food and water. The *Gclc* floxed mice in C57BL/6 genetic background was created by our group, as described in our previous report (*35*). The caspase 3 KO mice (006233) and caspase 1 KO mice (032662) were procured

from the Jackson Laboratory. Caspase 12 KO mice were purchased from Mutant Mouse Regional Resource Centers, while WT C57BL/6 mice were obtained from the National Institute of Aging.

D499E-Gclc KI mice

We introduced a specific mutation into the Gclc gene, converting aspartic acid to glutamic acid (GAC > GAA) at position 499. This genetic alteration led to the creation of D499E-Gclc KI (D499E-KI) mice using CRISPR technology, conducted by Applied StemCell located in Milpitas, California. No additional gene modifications, such as the addition or removal of restriction sites, were made. The Gclc.g2 guide RNA (gRNA), which targeted the mutation site, was used in conjunction with a single-stranded oligodeoxynucleotide (ssODN) donor molecule serving as an HDR (homology-directed repair) template to introduce the required point mutation (fig. S13). The process involved cytoplasmic microinjection of Gclc.g2 gRNA, ssODN, and Cas9 protein, followed by the identification of founder mice through DNA Sanger sequencing. Heterozygous D499E-KI mice were subsequently bred with WT C57BL/6J mice for a minimum of six generations. Subsequently, homozygous D499E-KI mice were produced by mating heterozygous D499E-KI individuals. Genomic DNA containing the GCLC gene was amplified from mouse tail genomic DNA extracts. The gene mutation was confirmed through Sanger DNA sequencing, with representative sequencing chromatograms provided in fig. S14. Colonies of homozygous D499E-KI mice within the C57BL/6 genetic background were consistently maintained throughout the duration of the study.

Mouse lens capsule explant culture and FGF-induced epithelial cell differentiation

Lens capsule culture was conducted using 2-month-old mice, following the procedures outlined in a previous publication (*21*). Briefly, a small incision was made at the posterior pole of the lens capsule. Subsequently, four to six flaps of the posterior capsule were delicately peeled from the posterior pore to the equator of the lens using fine forceps. The attached fibers were meticulously removed, and the lens capsule was then flattened and secured to the culture dish. The culture medium consisted of serum-free M199, supplemented with antibiotics and amphotericin B. Twenty-four hours after the initial culture, a final concentration of FGF-2 (200 ng/ml) was introduced, and the capsules were continuously cultured for an additional 48 hours. Capsules without FGF-2 served as the control group. Cell morphology was observed at 24-hour intervals, and at the end of the culture period, capsules were either fixed for immunofluorescence staining or lysed for immunoblotting assays.

Cell culture and treatment

The human lens epithelial cell line of FHL124 cells (obtained from M. Wormstone at the University of East Anglia, UK) (*74*) were cultured in minimum essential media supplemented with 5% fetal bovine serum (FBS), 2 mM glutamine, and penicillin/streptomycin (50 U/ml; HyClone, Cytiva) at 35°C in a humidified 5% CO_2 incubator. RPE, HeLa, HLE-B3, SW480, DLD1, and HEK293T cells were grown in Dulbecco's modified Eagle's medium (DMEM) with 10% FBS, 2 mM glutamine, and penicillin/streptomycin (50 U/ml; HyClone, Cytiva) at 37°C in a humidified 5% CO_2 incubator. MEF cells were cultured from WT and $Gclc^{fl/fl}$ E13.5 embryos following the protocol described in a previous report (*75*). Gclc KO MEF cells were generated by introducing stable Cre expression using retroviral particles carrying puromycin-resistant genes. MEF cells were cultured in DMEM medium with 10% FBS, 2 mM glutamine, and penicillin/streptomycin (50 U/ml; HyClone, Cytiva). In addition, 2 mM *N*-acetylcysteine was included in the culture medium and refreshed every 48 hours in Gclc KO MEF cells. To induce GCLC cleavage in FHL124 and MEF cells, overnight seeded cells were treated with 500 nM STS for 4 to 6 hours. For HeLa cells, overnight seeded cells were treated with TNFα (30 ng/ml) and CHX (10 μg/ml) for 4 to 6 hours to induce GCLC cleavage. Cells were then harvested at various time points as described in each assay.

Creating GCLC KO HeLa cells by CRISPR-Cas9 editing

The single guide RNA was successfully inserted into the lentiCRISPR v2 vector (a gift from F. Zhang, Addgene plasmid #52961). Lentiviral particles were then generated from HEK293T cells through cotransfection of lentiCRISPR v2, VSV-G, BH10 ϕ^{-}*env*$^{-}$, and pRev c (provided by J. Skowronski at Case Western Reserve University). Subsequently, FHL124 cells were infected with these lentiviral particles and allowed to grow for 48 hours. The stably infected cells were selected using puromycin (2 μg/ml). For single-cell expansion, the infected cells were diluted and plated in a 96-well plate. The individual clonal cell lines with GCLC deletion were validated through immunoblot analysis. Two sets of GCLC gRNA were used: GCLC gRNA1 with the sequence AGGCCAACATGCGAAAACGC and GCLC gRNA2 with the sequence AGAAATATCCGACATAGGAG.

Mammalian gene expression using retroviral particles and transient transfection

Human GCLM, GCLC (G73), and its truncated fragments G60 and G13 were cloned into pCG (*76*) expression vector. Both tag-free and N-terminal FLAG- and Myc-tagged expression vectors were used. For transient transfection, approximately 0.2×10^6 HeLa cells were seeded into a six-well plate at least 16 hours before the transfection. The plasmids were introduced into the cells using TransIT-LT1 reagent (Mirus Bio LLC) following the manufacturer's instructions. To achieve viral particle–based overexpression, tagged and tag-free G73, G60, and G13 were subcloned into the MSCV (puro) vector. Retroviral particles were produced from HEK293 cells, as previously described (*77*). For viral particle infection, FHL124 and HeLa cells were seeded overnight and then incubated with the viral particles for 48 hours, followed by puromycin selection. The gene expression of the stably infected cells was verified by immunoblot analysis, and the cells were cultured in the presence puromycin (2 μg/ml).

Mammalian ectopic protein expression

To achieve overexpression of the G13 fragment with the exact same amino acid sequence as the in vivo truncated form in cell culture, we used a ubiquitin fusion protein system at the N-terminal of the G13 protein. This system allowed the G13 fragment to be released by intracellular ubiquitin-specific proteases. We used a mutated form of ubiquitin (UbK48R) expression vector (*78*), provided by M. Scheffner from the University of Konstanz, Germany. The UbK48R-G13 construct was subcloned into the pCG expression vector containing a puromycin-resistant gene. Both transient transfection and generation of stably transfected cells were performed using the TransIT-LT1 reagent (Mirus Bio LLC)–mediated approach. To account for the potential impact of the ubiquitin fusion expression system, we also expressed G73 and G60 using the same system in all our ectopic expression experiments.

GSH assay

GSH levels were determined using the colorimetric assay method, as described in (*21*, *79*). Briefly, cultured cells and lenses were homogenized in an ice-cold mixture of 0.6% sulfosalicylic acid and freshly prepared 0.1 M potassium phosphate buffer with a pH of 7.5 and containing 5 mM EDTA. The resulting supernatant was used for the GSH assay. This assay involved the utilization of GR and β-NADPH enzymatic recycle colorimetric assay after derivatization by 5,5′-dithio-bis (2-nitrobenzoic acid).

Nondenaturing IP

The cells were collected and washed three times with ice-cold phosphate-buffered saline (PBS). Subsequently, they were lysed using a cell lysis buffer containing 20 mM tris-HCl (pH 7.5), 150 mM NaCl, 1 mM EDTA, 1 mM EGTA, and 1% Triton X-100, supplemented with protease inhibitors. To reduce nonspecific binding, the lysate was precleared by incubating it with protein A agarose resin at 4°C for 1 hour. After preclearing, the lysate was mixed with the primary antibody specific to the protein of interest, protein A resin, and gently rotated for 2 hours at 4°C. The protein A resin was washed five times with the cell lysis buffer to remove any nonspecifically bound proteins. Subsequently, the target protein was released from the protein A resin by incubating the beads in 2× Laemmli SDS sample buffer for 10 min at 95°C. This allowed for the elution of the immunoprecipitated protein for downstream analysis.

IP under denaturing conditions and G60 separation

To perform the denaturing IP and pull down the G60 fragment, the following steps were carried out. A pool of 114 lenses older than 8 months was homogenized in 11.4-ml denaturing lysis buffer (pH 7.4), which contained 1% SDS, 5 mM EDTA, 10 mM dithiothreitol, and proteinase inhibitors. The lysate was incubated at 95°C for 5 min and then diluted 10 times with cell lysis buffer [20 mM tris-HCl (pH 7.5), 150 mM NaCl, 1 mM EDTA, 1 mM EGTA, and 1% Triton X-100] and incubated on ice for 5 min. The supernatant obtained after spinning at 21,000*g* for 15 min at 4°C was further concentrated using a 10-kDa cutoff centricon. The concentrated lysate was mixed with the GCLC antibody (ab190685, Abcam, Boston, MA) and incubated for 16 hours at 4°C with gentle rotation. Subsequently, protein A beads were added to the mixture and incubated for an additional 16 hours at 4°C with gentle rotation. The protein A beads were pelleted after centrifugation and then washed six times with the cell lysis buffer containing protease inhibitors. To release the G60 fragment, 200 μl of 2× Laemmli SDS sample buffer was added to the protein A beads and incubated for 10 min at 95°C.

For mass spectrometry analysis, the eluted samples were separated by SDS–polyacrylamide gel electrophoresis (SDS-PAGE) using PROTEAN II XL Cell (18.5 × 20 cm, Bio-Rad, Hercules, CA). The G73 and G60 protein bands were visualized by staining with Bio-Safe Coomassie (161-078, Bio-Rad) and then excised for protein extraction and mass spectrometry analysis.

Mass spectrometry to determine GCLC cleavage site

The gel bands were digested using a ProGest robot (DigiLab). Briefly, the gel bands were washed with 25 mM ammonium bicarbonate followed by acetonitrile. The protein was then reduced with 10 mM dithiothreitol at 60°C and subsequently alkylated with 50 mM iodoacetamide at room temperature. The digestion was carried out using trypsin (Promega) at 37°C for 4 hours. After digestion, the peptides were extracted with formic acid, and the supernatant was directly analyzed without further processing. The gel digests were subjected to analysis by nano LC–tandem mass spectrometry (LC-MS/MS) using a Waters NanoAcquity high-performance liquid chromatography system interfaced with a Thermo Fisher Scientific Q Exactive mass spectrometer. Peptides were loaded onto a trapping column and eluted over a 75-μm analytical column, both packed with Luna C18 resin (Phenomenex), at a flow rate of 350 nl/min.

The mass spectrometer was operated in data-dependent mode, performing MS and MS/MS in the Orbitrap at 70,000 full width at half maximum (FWHM) resolution and 17,500 FWHM resolution, respectively. The 15 most abundant ions were selected for MS/MS. Data were searched using Mascot with a peptide tolerance of 10 parts per million, fragment mass tolerance of 0.02 Da, and a maximum of two missed cleavages.

Protein structure and protein complex prediction by AlphaFold and AlphaFold-multimer

We used both AlphaFold2 and AlphaFold-multimer 2 on UCSF ChimeraX, a software developed by the Resource for Biocomputing, Visualization, and Informatics at the University of California (*80*). We input the amino acid sequences of human GCLC(G73) and its truncated fragments, G60 and G13, for protein structure prediction. In addition, we used the amino acid sequence of human GCLM to predict the protein complexes between GCLM and G73, G60, G13, as well as the combination of G60 and G13.

Human and mouse lens dissection for protein spatial distribution studies

For the spatial distribution study, human lenses were carefully dissected into several layers, progressing from the capsule to the nucleus. The average size of the human lens in our study was approximately 8 mm in diameter. Once the lens capsule was removed, we selectively peeled approximately 1-mm-sized fiber cells in each fraction, designating them as cortex 1 to 3. The remaining core section, which was about 5 mm in size, was analyzed as the lens nucleus.

As for mouse lenses, we adhered to the established procedure for isolating capsules and fibers (*77*).

GCL enzymatic activity assay using LC-MS method

We have developed a method for measuring GCL activity in both cell culture and lens tissues using LC-MS, building on previous research. The method is briefly described as follows:

Initially, a cell pellet or lens tissue is homogenized in a mixture containing 25 mM tris, 150 mM KCl, 20 mM $MgCl_2$, and 2 mM EDTA, and pH was adjusted at pH 8.6 with NH_4OH. This is done on ice and followed by a sonication process for 40 s, with 5 s on and 5 s off intervals. A 10-μl sample of the supernatant is then incubated with 70-μl freshly prepared reaction buffer. The reaction buffer contains 5.6 mM ATP, 2.1 mM phosphoenolpyruvate, 5 μM benzylamine hydrochloride, pyruvate kinase (30,000 U/liter), and 40 mM glutamate. The preincubation period lasts for 2 min at a temperature of 37°C. The reaction is initiated by adding 20 μl of 20 mM L-2-aminobutyric acid, with the incubation period extending for another 15 to 45 min. The reaction is subsequently halted by introducing 40 μl of 6% sulfosalicylic acid. The reaction mixture is then centrifuged at a speed of 21,000*g* for a duration of 5 min at 4°C. The supernatant from this centrifugation is subjected to LC-MS analysis. γ-Glutamylaminobutyric acid (GGAB) is used as a standard, while benzylamine serves as the internal standard (IS).

For sample separation and analysis, sample separation was executed on a Shimadzu Nexera UHPLC system using a Phenomenex Kinetex C18 column (100 mm by 2.1 mm, 1.7 um). The procedure maintained a flow rate of 0.16 ml/min, transitioning from 1 to 80% acetonitrile (supplemented with 0.1% formic acid) over 5 min. The entire analysis spanned 10 min. The effluent underwent ionization through ion electrospray in a positive mode, using a TSQ Quantiva triple-quadrupole mass spectrometer, with the following settings: ion spray voltage: 3500 V, sheath gas: 35, ion transfer tube temperature: 325°C, aux gas: 10, FWHM: 0.7 for Q1/Q3 resolution. Commercial standards were used to ascertain the ideal collision energy and radio frequency (RF) lens. For the compounds GGAB and benzylamine (IS), transitions 233.0/104.1 and 108.3/65.1 were observed, respectively. The peak areas for these transitions across samples were computed using Skyline software (version 20.0, University of Washington).

White and red blood cell isolation

One millilter of mouse blood was collected via cardiac puncture and combined with 0.1 ml of EDTA (20 mg/ml) (pH 8.0). Following centrifugation at 400*g* for 10 min at room temperature, the blood separated into three distinct layers. The white blood cells were found in the middle layer, while the red blood cells settled in the bottom layer. Both white and red blood cells were transferred to a fresh tube and rinsed twice with PBS. Subsequently, the cells were lysed using a cell lysis buffer composed of 20 mM tris-HCl (pH 7.5), 150 mM NaCl, 1 mM EDTA, 1 mM EGTA, and 1% Triton X-100. The resultant supernatant was then analyzed using an immunoblotting assay.

Calpain digestion

To optimize the digestion conditions for calpain-1, we used the fluorogenic calpain substrate III. The efficiency of calpain-1 digestion was monitored by measuring the maximum fluorescence production. These optimized digestion conditions were subsequently applied to the GCLC cleavage test. For the GCLC digestion, 50 μg of recombinant human GCLC was combined with 1 milliunit of calpain-1 in a digestion buffer comprising 50 mM tris-HCl, 50 mM NaCl, 0.25 mM $CaCl_2$, and 5% glycerol, all maintained at 37°C for 1 hour. The resulting protein was then subjected to an immunoblotting assay. A calpain inhibitor III, at a concentration of 5 nM, was used to inhibit calpain digestion.

Lens opacity analysis by the slit lamp

The lens opacity was assessed using a slit lamp (SL-D4, Topcon, Livermore, CA) with ×40 magnification. The severity of cataract was categorized into three grades: grade I denoting no cataract, grade II indicating mild cataract, and grade III representing severe cataract. Mice aged 20 months were included in the study, and any mice exhibiting corneal opacity were excluded from the cohort. To facilitate the examination, a mydriatic eye drop (0.5% tropicamide ophthalmic solution, catalog no. NDC 1748-101-12, Akorn, Lake Forest, IL) was administered 5 min before the slit lamp recording. Throughout the procedure, mice were anesthetized with isoflurane (catalog no. 46066-755-04, Aspen Veterinary Resources, Liberty, MO).

Dark-field, grid view microscopy, and lens capsule and fiber phase contrast microscopy

Dark-field images of the lens were acquired in accordance with the methods described in a previous publication (*81*). For lens grid view microscopy, we followed the procedures outlined in another prior publication (*82*). Briefly, the lenses were incubated in prewarmed Hanks' balanced salt solution. Each lens was positioned with its anterior side facing a copper electron microscope specimen grid and then imaged using a Leica M80 microscope (Leica, Buffalo Grove, IL). Subsequently, the lenses were inverted to have the anterior side facing up, and dark-field images were captured without the electron microscope specimen grid. Following this, the lenses were dissected to isolate the lens capsule and fiber mass, and phase contrast images of both components were obtained.

TUNEL staining and quantification

The paraffin-embedded sections underwent deparaffinization and followed standard rehydration procedures. Staining steps were performed in accordance with the manufacturer's instructions. To quantify TUNEL-positive cells, three consecutive sections from a single lens were examined. The average count of TUNEL-positive dots from these three sections was regarded as representative of one lens. In total, the analysis included four lenses from four different mice.

Immunoblot assay

Immunoblot assays were performed as previously described (*83*). Briefly, the protein concentration from the supernatant was measured by protein bicinchoninic acid assay (Thermo Fisher Scientific). Equal amounts of protein were subjected to appropriate SDS-PAGE gel electrophoresis and transferred to a 0.45–μm–pore size polyvinylidene difluoride membrane. Detection was done using the enhanced chemiluminescence Western blotting detection system. All antibodies used in this study are listed in table S1.

Confocal microscope

All images were captured by a Leica STELLARIS confocal microscopy and analyzed by the LAS X Life Science Microscope Software.

Statistical analysis

The experiments were repeated at least three times, and the specific sample size (n) for each experiment is indicated in the corresponding figure legend. All statistical analyses were conducted using GraphPad Prism 10.0.1 software. For multiple group comparisons, analysis of variance (ANOVA) with post hoc Tukey test was used, while t tests were used for comparisons between two groups. The chi-square test was used to compare cataract prevalence among the groups. In addition, a Mann-Whitney test was used to compare cataract area and density between each group. The data are presented as mean ± SD. A significance level of $P \leq 0.05$ was considered statistically significant. The levels of significance are denoted by asterisks ($^{*}P \leq 0.05$; $^{**}P \leq 0.01$; $^{***}P \leq 0.001$; $^{****}P \leq 0.0001$).

Supplementary Materials

This PDF file includes:

Figs. S1 to S14

Table S1

REFERENCES AND NOTES

1. M. V. Cicinelli, J. C. Buchan, M. Nicholson, V. Varadaraj, R. C. Khanna, Cataracts. *Lancet* **401**, 377–389 (2023).
2. GBD 2019 Blindness and Vision Impairment Collaborators; Vision Loss Expert Group of the Global Burden of Disease Study, Causes of blindness and vision impairment in 2020 and trends over 30 years, and prevalence of avoidable blindness in relation to VISION

2020: The Right to Sight: An analysis for the Global Burden of Disease Study. *Lancet Glob. Health* **9**, e144–e160 (2021).
3. Y. C. Liu, M. Wilkins, T. Kim, B. Malyugin, J. S. Mehta, Cataracts. *Lancet* **390**, 600–612 (2017).
4. I. M. Wormstone, Y. M. Wormstone, A. J. O. Smith, J. A. Eldred, Posterior capsule opacification: What's in the bag? *Prog. Retin. Eye Res.* **82**, 100905 (2021).
5. Z. Wei, P. Gordon, C. Hao, J. Huangfu, E. Fan, X. Zhang, H. Yan, X. Fan, Aged lens epithelial cells suppress proliferation and epithelial-mesenchymal transition-relevance for posterior capsule opacification. *Cells* **11**, (2022).
6. D. D. Koch, T. Kohnen, Retrospective comparison of techniques to prevent secondary cataract formation after posterior chamber intraocular lens implantation in infants and children. *J Cataract Refract Surg* **23**, 657–663 (1997).
7. A. Vasavada, H. Chauhan, Intraocular lens implantation in infants with congenital cataracts. *J Cataract Refract Surg* **20**, 592–598 (1994).
8. G. Brian, H. Taylor, Cataract blindness--challenges for the 21st century. *Bull. World Health Organ.* **79**, 249–256 (2001).
9. C. A. McCarty, M. B. Nanjan, H. R. Taylor, Attributable risk estimates for cataract to prioritize medical and public health action. *Invest. Ophthalmol. Vis. Sci.* **41**, 3720–3725 (2000).
10. N. Hatsusaka, N. Yamamoto, H. Miyashita, E. Shibuya, N. Mita, M. Yamazaki, T. Shibata, H. Ishida, Y. Ukai, E. Kubo, H. M. Cheng, H. Sasaki, Association among pterygium, cataracts, and cumulative ocular ultraviolet exposure: A cross-sectional study in Han people in China and Taiwan. *PLOS ONE* **16**, e0253093 (2021).
11. R. A. Quinlan, J. I. Clark, Insights into the biochemical and biophysical mechanisms mediating the longevity of the transparent optics of the eye lens. *J. Biol. Chem.* **298**, 102537 (2022).
12. X. Fan, V. M. Monnier, Protein posttranslational modification (PTM) by glycation: Role in lens aging and age-related cataractogenesis. *Exp. Eye Res.* **210**, 108705 (2021).
13. K. K. Sharma, P. Santhoshkumar, Lens aging: Effects of crystallins. *Biochim. Biophys. Acta* **1790**, 1095–1108 (2009).
14. B. K. Derham, J. J. Harding, Alpha-crystallin as a molecular chaperone. *Prog. Retin. Eye Res.* **18**, 463–509 (1999).
15. R. H. Nagaraj, M. Linetsky, A. W. Stitt, The pathogenic role of Maillard reaction in the aging eye. *Amino Acids* **42**, 1205–1220 (2012).
16. K. J. Lampi, P. A. Wilmarth, M. R. Murray, L. L. David, Lens β-crystallins: The role of deamidation and related modifications in aging and cataract. *Prog. Biophys. Mol. Biol.* **115**, 21–31 (2014).
17. R. J. Truscott, M. G. Friedrich, The etiology of human age-related cataract. Proteins don't last forever. *Biochim. Biophys. Acta* **1860**, 192–198 (2016).
18. F. Y. Liu, J. L. Fu, L. Wang, Q. Nie, Z. Luo, M. Hou, Y. Yang, X. D. Gong, Y. Wang, Y. Xiao, J. Xiang, X. Hu, L. Zhang, M. Wu, W. Chen, B. Cheng, L. Luo, X. Zhang, X. Liu, D. Zheng, S. Huang, Y. Liu, D. W. Li, Molecular signature for senile and complicated cataracts derived from analysis of sumoylation enzymes and their substrates in human cataract lenses. *Aging Cell* **19**, e13222 (2020).
19. N. Fujii, T. Takata, N. Fujii, K. Aki, H. Sakaue, D-Amino acids in protein: The mirror of life as a molecular index of aging. *Biochim. Biophys. Acta Proteins Proteom.* **1866**, 840–847 (2018).
20. D. Borchman, M. C. Yappert, Lipids and the ocular lens. *J. Lipid Res.* **51**, 2473–2488 (2010).
21. Z. Wei, C. Hao, J. Huangfu, R. Srinivasagan, X. Zhang, X. Fan, Aging lens epithelium is susceptible to ferroptosis. *Free Radic. Biol. Med.* **167**, 94–108 (2021).
22. M. F. Lou, Glutathione and glutaredoxin in redox regulation and cell signaling of the lens. *Antioxidants (Basel)* **11**, (2022).
23. D. C. Beebe, N. M. Holekamp, Y. B. Shui, Oxidative damage and the prevention of age-related cataracts. *Ophthalmic Res.* **44**, 155–165 (2010).
24. R. J. Truscott, Age-related nuclear cataract-oxidation is the key. *Exp. Eye Res.* **80**, 709–725 (2005).
25. J. R. Hughes, V. A. Levchenko, S. J. Blanksby, T. W. Mitchell, A. Williams, R. J. Truscott, No turnover in lens lipids for the entire human lifespan. *eLife* **4**, e06003 (2015).
26. W. G. Chaney, A. Spector, HPLC analysis of lens GSH and GSSG. *Curr. Eye Res.* **3**, 345–350 (1984).
27. X. Fan, V. M. Monnier, J. Whitson, Lens glutathione homeostasis: Discrepancies and gaps in knowledge standing in the way of novel therapeutic approaches. *Exp. Eye Res.* **156**, 103–111 (2017).
28. V. N. Reddy, N. J. Unakar, Localization of gamma-glutamyl transpeptidase in rabbit lens, ciliary process and cornea. *Exp. Eye Res.* **17**, 405–408 (1973).
29. L. L. Ross, L. Barber, S. S. Tate, A. Meister, Enzymes of the gamma-glutamyl cycle in the ciliary body and lens. *Proc. Natl. Acad. Sci. U.S.A.* **70**, 2211–2214 (1973).
30. J. B. Mackic, R. Kannan, N. Kaplowitz, B. V. Zlokovic, Low de novo glutathione synthesis from circulating sulfur amino acids in the lens epithelium. *Exp. Eye Res.* **64**, 615–626 (1997).
31. B. Li, L. Li, P. J. Donaldson, J. C. Lim, Dynamic regulation of GSH synthesis and uptake pathways in the rat lens epithelium. *Exp. Eye Res.* **90**, 300–307 (2010).
32. J. A. Whitson, D. R. Sell, M. C. Goodman, V. M. Monnier, X. Fan, Evidence of dual mechanisms of glutathione uptake in the rodent lens: A novel role for vitreous humor in lens glutathione homeostasis. *Invest. Ophthalmol. Vis. Sci.* **57**, 3914–3925 (2016).
33. H. I. Calvin, C. Medvedovsky, B. V. Worgul, Near-total glutathione depletion and age-specific cataracts induced by buthionine sulfoximine in mice. *Science* **233**, 553–555 (1986).
34. H. I. Calvin, S. von Hagen, J. L. Hess, S. A. Patel, S. C. Fu, Lens GSH depletion and electrolyte changes preceding cataracts induced by buthionine sulfoximine in suckling mice. *Exp. Eye Res.* **54**, 621–626 (1992).
35. X. Fan, X. Liu, S. Hao, B. Wang, M. L. Robinson, V. M. Monnier, The LEGSKO mouse: A mouse model of age-related nuclear cataract based on genetic suppression of lens glutathione synthesis. *PLOS ONE* **7**, e50832 (2012).
36. F. J. Giblin, Glutathione: A vital lens antioxidant. *J. Ocul. Pharmacol. Ther.* **16**, 121–135 (2000).
37. H. E. Henkes, On the distribution of glutathione and vitamin C in the lens and cornea. *Ophthalmologica* **112**, 113–128 (1946).
38. Y. Chen, H. G. Shertzer, S. N. Schneider, D. W. Nebert, T. P. Dalton, Glutamate cysteine ligase catalysis: Dependence on ATP and modifier subunit for regulation of tissue glutathione levels. *J. Biol. Chem.* **280**, 33766–33774 (2005).
39. W. B. Rathbun, Lenticular glutathione synthesis: Rate-limiting factors in its regulation and decline. *Curr. Eye Res.* **3**, 101–108 (1984).
40. C. C. Franklin, C. M. Krejsa, R. H. Pierce, C. C. White, N. Fausto, T. J. Kavanagh, Caspase-3-dependent cleavage of the glutamate-L-cysteine ligase catalytic subunit during apoptotic cell death. *Am. J. Pathol.* **160**, 1887–1894 (2002).
41. M. Gao, Y. Huang, L. Wang, M. Huang, F. Liu, S. Liao, S. Yu, Z. Lu, S. Han, X. Hu, Z. Qu, X. Liu, T. Assefa Yimer, L. Yang, Z. Tang, D. W. Li, M. Liu, HSF4 regulates lens fiber cell differentiation by activating p53 and its downstream regulators. *Cell Death Dis.* **8**, e3082 (2017).
42. S. Basu, S. Rajakaruna, A. De Arcangelis, L. Zhang, E. Georges-Labouesse, A. S. Menko, α6 integrin transactivates insulin-like growth factor receptor-1 (IGF-1R) to regulate caspase-3-mediated lens epithelial cell differentiation initiation. *J. Biol. Chem.* **289**, 3842–3855 (2014).
43. S. Basu, S. Rajakaruna, A. S. Menko, Insulin-like growth factor receptor-1 and nuclear factor κB are crucial survival signals that regulate caspase-3-mediated lens epithelial cell differentiation initiation. *J. Biol. Chem.* **287**, 8384–8397 (2012).
44. G. F. Weber, A. S. Menko, The canonical intrinsic mitochondrial death pathway has a non-apoptotic role in signaling lens cell differentiation. *J. Biol. Chem.* **280**, 22135–22145 (2005).
45. T. R. Shearer, H. Ma, M. Shih, C. Fukiage, M. Azuma, Calpains in the lens and cataractogenesis. *Methods Mol. Biol.* **144**, 277–285 (2000).
46. S. Biswas, F. Harris, S. Dennison, J. Singh, D. A. Phoenix, Calpains: Targets of cataract prevention? *Trends Mol. Med.* **10**, 78–84 (2004).
47. L. J. Robertson, L. L. David, M. A. Riviere, P. A. Wilmarth, M. S. Muir, J. D. Morton, Susceptibility of ovine lens crystallins to proteolytic cleavage during formation of hereditary cataract. *Invest. Ophthalmol. Vis. Sci.* **49**, 1016–1022 (2008).
48. Q. Yan, J. P. Liu, D. W. Li, Apoptosis in lens development and pathology. *Differentiation* **74**, 195–211 (2006).
49. Z. Liu, S. Huang, Y. Zheng, T. Zhou, L. Hu, L. Xiong, D. W. Li, Y. Liu, The lens epithelium as a major determinant in the development, maintenance, and regeneration of the crystalline lens. *Prog. Retin. Eye Res.* **92**, 101112 (2023).
50. P. Schook, Morphogenetic movements during the early development of the chick eye. An ultrastructural and spatial study. C. Obliteration of the lens stalk lumen and separation of the lens vesicle from the surface ectoderm. *Acta Morphol. Neerl. Scand.* **18**, 195–201 (1980).
51. C. C. Franklin, D. S. Backos, I. Mohar, C. C. White, H. J. Forman, T. J. Kavanagh, Structure, function, and post-translational regulation of the catalytic and modifier subunits of glutamate cysteine ligase. *Mol. Aspects Med.* **30**, 86–98 (2009).
52. J. I. Lee, J. Kang, M. H. Stipanuk, Differential regulation of glutamate-cysteine ligase subunit expression and increased holoenzyme formation in response to cysteine deprivation. *Biochem. J.* **393**, 181–190 (2006).
53. Y. Yang, M. Z. Dieter, Y. Chen, H. G. Shertzer, D. W. Nebert, T. P. Dalton, Initial characterization of the glutamate-cysteine ligase modifier subunit Gclm(−/−) knockout mouse. Novel model system for a severely compromised oxidative stress response. *J. Biol. Chem.* **277**, 49446–49452 (2002).
54. M. Zhu, G. T. Bowden, Molecular mechanism(s) for UV-B irradiation-induced glutathione depletion in cultured human keratinocytes. *Photochem. Photobiol.* **80**, 191–196 (2004).
55. R. M. Liu, P. K. Vayalil, C. Ballinger, D. A. Dickinson, W. T. Huang, S. Wang, T. J. Kavanagh, Q. L. Matthews, E. M. Postlethwait, Transforming growth factor β suppresses glutamate-cysteine ligase gene expression and induces oxidative stress in a lung fibrosis model. *Free Radic. Biol. Med.* **53**, 554–563 (2012).
56. D. J. van den Dobbelsteen, C. S. Nobel, J. Schlegel, I. A. Cotgreave, S. Orrenius, A. F. Slater, Rapid and specific efflux of reduced glutathione during apoptosis induced by anti-Fas/APO-1 antibody. *J. Biol. Chem.* **271**, 15420–15427 (1996).
57. R. Franco, J. A. Cidlowski, SLCO/OATP-like transport of glutathione in FasL-induced apoptosis: Glutathione efflux is coupled to an organic anion exchange and is necessary

for the progression of the execution phase of apoptosis. *J. Biol. Chem.* **281**, 29542–29557 (2006).
58. T. Siitonen, P. Alaruikka, P. Mantymaa, E. R. Savolainen, T. J. Kavanagh, C. M. Krejsa, C. C. Franklin, V. Kinnula, P. Koistinen, Protection of acute myeloblastic leukemia cells against apoptotic cell death by high glutathione and gamma-glutamylcysteine synthetase levels during etoposide-induced oxidative stress. *Ann. Oncol.* **10**, 1361–1367 (1999).
59. M. F. Lou, Redox regulation in the lens. *Prog. Retin. Eye Res.* **22**, 657–682 (2003).
60. R. Folberg, The eye, W. H. Spencer, *Ophthalmic Pathology. An Atlas and Testbook*, (W.B. Saunders, Co., ed. 4 1996).
61. H. E. Grossniklaus, J. M. Nickerson, H. F. Edelhauser, L. A. Bergman, L. Berglin, Anatomic alterations in aging and age-related diseases of the eye. *Invest. Ophthalmol. Vis. Sci.* **54**, ORSF23-27 (2013).
62. M. H. Sweeney, R. J. Truscott, An impediment to glutathione diffusion in older normal human lenses: A possible precondition for nuclear cataract. *Exp. Eye Res.* **67**, 587–595 (1998).
63. R. J. Truscott, Age-related nuclear cataract: A lens transport problem. *Ophthalmic Res.* **32**, 185–194 (2000).
64. K. R. Heys, S. L. Cram, R. J. Truscott, Massive increase in the stiffness of the human lens nucleus with age: The basis for presbyopia? *Mol. Vis.* **10**, 956–963 (2004).
65. K. R. Heys, R. J. Truscott, The stiffness of human cataract lenses is a function of both age and the type of cataract. *Exp. Eye Res.* **86**, 701–703 (2008).
66. D. C. Beebe, N. M. Holekamp, C. Siegfried, Y. B. Shui, Vitreoretinal influences on lens function and cataract. *Philos. Trans. R. Soc. Lond. B Biol. Sci.* **366**, 1293–1300 (2011).
67. X. Fan, S. Zhou, B. Wang, G. Hom, M. Guo, B. Li, J. Yang, D. Vaysburg, V. M. Monnier, Evidence of highly conserved β-crystallin disulfidome that can be mimicked by in vitro oxidation in age-related human cataract and glutathione depleted mouse lens. *Mol. Cell Proteomics* **14**, 3211–3223 (2015).
68. X. Fan, L. W. Reneker, M. E. Obrenovich, C. Strauch, R. Cheng, S. M. Jarvis, B. J. Ortwerth, V. M. Monnier, Vitamin C mediates chemical aging of lens crystallins by the Maillard reaction in a humanized mouse model. *Proc. Natl. Acad. Sci. U.S.A.* **103**, 16912–16917 (2006).
69. A. V. Katta, R. V. Katkam, H. Geetha, Lipid peroxidation and the total antioxidant status in the pathogenesis of age related and diabetic cataracts: A study on the lens and blood. *J. Clin. Diagn. Res.* **7**, 978–981 (2013).
70. X. Zhu, A. Korlimbinis, R. J. Truscott, Age-dependent denaturation of enzymes in the human lens: A paradigm for organismic aging? *Rejuvenation Res.* **13**, 553–560 (2010).
71. M. Wei, K. Y. Xing, Y. C. Fan, T. Libondi, M. F. Lou, Loss of thiol repair systems in human cataractous lenses. *Invest. Ophthalmol. Vis. Sci.* **56**, 598–605 (2015).
72. M. F. Lou, G. T. Xu, X. L. Cui, Further studies on the dynamic changes of glutathione and protein-thiol mixed disulfides in H2O2 induced cataract in rat lenses: Distributions and effect of aging. *Curr. Eye Res.* **14**, 951–958 (1995).
73. M. F. Lou, Thiol regulation in the lens. *J. Ocul. Pharmacol. Ther.* **16**, 137–148 (2000).
74. L. C. B. Reddan, J. R. Hitt, A. L. M. Bagchi, E. M. Raphtis, J. T. Pena, D. C. Dziedzic, Generation of two non-transfected human lens cell lines. *Invest. Ophthalmol. Vis. Sci.* **40**, S970–S970 (1999).
75. Y. S. Tan, Y. L. Lei, Generation and culture of mouse embryonic fibroblasts. *Methods Mol. Biol.* **1960**, 85–91 (2019).
76. M. Tanaka, W. Herr, Differential transcriptional activation by Oct-1 and Oct-2: Interdependent activation domains induce Oct-2 phosphorylation. *Cell* **60**, 375–386 (1990).
77. J. Huangfu, C. Hao, Z. Wei, I. M. Wormstone, H. Yan, X. Fan, Cellular FLICE-like inhibitory protein (cFLIP) critically maintains apoptotic resistance in human lens epithelial cells. *Cell Death Dis.* **12**, 386 (2021).
78. K. Matentzoglu, M. Scheffner, Ubiquitin-fusion protein system: A powerful tool for ectopic protein expression in mammalian cells. *Biotechniques* **46**, 21–22 (2009).
79. I. Rahman, A. Kode, S. K. Biswas, Assay for quantitative determination of glutathione and glutathione disulfide levels using enzymatic recycling method. *Nat. Protoc.* **1**, 3159–3165 (2006).
80. E. F. Pettersen, T. D. Goddard, C. C. Huang, E. C. Meng, G. S. Couch, T. I. Croll, J. H. Morris, T. E. Ferrin, U. C. S. F. ChimeraX, UCSF ChimeraX: Structure visualization for researchers, educators, and developers. *Protein Sci.* **30**, 70–82 (2021).
81. Z. Wei, C. Hao, R. Srinivasagan, H. Wu, J. K. Chen, X. Fan, Mitotic activation around wound edges and epithelialization repair in UVB-induced capsular cataracts. *Invest. Ophthalmol. Vis. Sci.* **62**, 29 (2021).
82. K. Varadaraj, P. G. FitzGerald, S. S. Kumari, Deletion of beaded filament proteins or the C-terminal end of Aquaporin 0 causes analogous abnormal distortion aberrations in mouse lens. *Exp. Eye Res.* **209**, 108645 (2021).
83. Z. Wei, J. Caty, J. Whitson, A. D. Zhang, R. Srinivasagan, T. J. Kavanagh, H. Yan, X. Fan, Reduced glutathione level promotes epithelial-mesenchymal transition in lens epithelial cells via a Wnt/β-catenin–mediated pathway. *Am. J. Pathol.* **187**, 2399–2412 (2017).

Acknowledgments: We are very thankful to D. Kumiski at Augusta University EM/Histology Core for helping with tissue processing and sectioning. We extend our gratitude to M. Deshmukh and N. Hondrogiannis at the University of North Carolina-Chapel Hill for contribution of caspase 6 KO mouse eye tissue. We appreciate W. Zhi at Augusta University Proteomics Core for helping with the LC-MS study. **Funding:** This research was supported by grants from EY028158 (X.F.), EY032488 (X.F.), the James Fickel Alzheimer's Disease Research Fund MCGFD01043 (X.F.), and NEI Center Core Grant for Vision Research (P30EY031631) at Augusta University. Molecular graphics and analyses performed with UCSF ChimeraX (*80*), developed by the Resource for Biocomputing, Visualization, and Informatics at the University of California, San Francisco, with support from National Institutes of Health R01-GM129325 and the Office of Cyber Infrastructure and Computational Biology, National Institute of Allergy and Infectious Diseases. **Author contributions:** X.F. conceived the research; S.S., C.H., K.R.R., M.E.M.-L., J.-K.C., and V.M.M. provided critical ideas for the design of this study; Z.W., C.H., K.R.R., X.F., and R.S. acquired the data; C.H., S.S., V.M.M., M.W.H., X.F., and M.E.M.-L. contributed critical materials; X.F. and V.M.M. supervised the research; Z.W., C.H., K.R.R., R.S., J.-K.C., and X.F. analyzed and interpreted the data; X.F. wrote the manuscript; V.M.M., S.S., M.E.M.-L., and J.-K.C. provided assistance with editing. All authors critically reviewed and provided input to the manuscript. **Competing interests:** The authors declare that they have no competing interests. **Data and materials availability:** All data needed to evaluate the conclusions in the paper are present in the paper and/or the Supplementary Materials. Request for the D499E-KI mice should be submitted to X.F. at xfan@augusta.edu.

Submitted 28 September 2023
Accepted 22 March 2024
Published 26 April 2024
10.1126/sciadv.adl1088